RSC Sustainability

ROYAL SOCIETY OF CHEMISTRY

PAPER

View Article Online
View Journal | View Issue

Cite this: *RSC Sustainability*, 2026, **4**, 2232

Aerobic titania photocatalysis: selective oxidative dehydrogenation of tetrahydroisoquinoline and related amines†

Paula Romero-Navarro, [a] Iris Martín-García, [a] Anabel Lanterna, ‡[b] Juan C. Scaiano [b] and Francisco Alonso *[a]

3,4-Dihydroisoquinolines are high-value chemicals, both as medicinally relevant compounds and as intermediates for the synthesis of 1,2,3,4-tetrahydroisoquinoline derivatives, which are widely regarded as privileged scaffolds in drug discovery. Though envisaged as a direct route, the partial oxidation of 1,2,3,4-tetrahydroisoquinolines to 3,4-dihydroisoquinolines is, however, very challenging due to the inherent tendency of these substrates toward over-oxidation to the aromatic isoquinolines. Herein, we have used 1,2,3,4-tetrahydroisoquinoline (THIQ) as a model substrate for its selective oxidative dehydrogenation to 3,4-dihydroisoquinoline (DHIQ) under heterogeneous photochemical conditions with titania-based photocatalysts. Among the materials tested, TiO_2-P25 and CuNPs/TiO_2-P25 have been found to be the best photocatalysts in terms of conversion and selectivity upon irradiation (369 nm) in acetonitrile, with oxygen as a terminal oxidant. Notably, high conversion and selectivity were also attained with TiO_2-P25 in the presence of Cs_2CO_3 under air. Although pristine TiO_2-P25 represents the simplest and most readily available photocatalyst, CuNPs/TiO_2-P25 is clearly superior from a reusability standpoint, maintaining high conversions (97–96%) and excellent selectivities (97:3–96:4) over the first four cycles, and consistently outperforming TiO_2-P25 in the oxidation of other amines. A detailed characterisation of this catalyst, combined with comprehensive mechanistic studies, supports a strong substrate-surface interaction that facilitates single-electron transfer oxidation of the former; accordingly, a consistent reaction mechanism has been proposed. A meticulous green chemistry assessment shows that, while TiO_2-P25 displays the most favourable risk-factor score, CuNPs/TiO_2-P25 provides the most balanced overall sustainability profile when risk factors, waste generation and recyclability are considered, and benchmarks favourably against previously reported photocatalytic methodologies. Overall, this study introduces an efficient and sustainable photocatalytic method that not only overcomes key limitations of previous systems, but also underscores the effectiveness and practicality of heterogeneous photochemical approaches under mild aerobic conditions.

Received 24th March 2026
Accepted 7th April 2026

DOI: 10.1039/d6su00169f

rsc.li/rscsus

Sustainability spotlight

Sustainable chemical production requires oxidations that minimise waste and hazardous reagents. Using molecular oxygen as the sole terminal oxidant, we report a heterogeneous photocatalytic dehydrogenation that converts tetrahydroisoquinolines and related amines to valuable imines while suppressing over-oxidation. A simple CuNPs/TiO_2-P25 photocatalyst combines high chemoselectivity with reuse over multiple cycles and enables 80% solvent recovery. An evidence-based assessment (*E*-factor ≈ 5, energy demand and risk-factor analysis covering catalyst preparation and use) provides transparent comparison with representative literature methods. Primary contribution to UN SDGs: SDG 12 (responsible consumption and production); secondary links: SDG 9 (innovation in sustainable chemical processes) and SDG 13 (reduced waste/energy demand supporting lower emissions).

Introduction

Imines (Schiff bases)[1] possess a versatile carbon-nitrogen double bond which can undergo a variety of useful organic transformations,[2] but can also be used as building blocks for covalent organic frameworks and for metal complexation in homogeneous and heterogeneous catalysis.[3] They are not only the immediate precursors of amines but key intermediates in

[a]*Instituto de Síntesis Orgánica (ISO) and Departamento de Química Orgánica, Facultad de Ciencias, Universidad de Alicante, Apdo. 99, 03080 Alicante, Spain. E-mail: falonso@ua.es*

[b]*Department of Chemistry and Biomolecular Sciences and Centre for Catalysis Research and Innovation, University of Ottawa, 10 Marie Curie, Ottawa, Ontario K1N 6N5, Canada*

† Dedicated to the memory of Professor Veselin Kmetov.

‡ Present address: School of Chemistry, Faculty of Science, University of Nottingham, University Park, Nottingham NG7 2RD, United Kingdom.

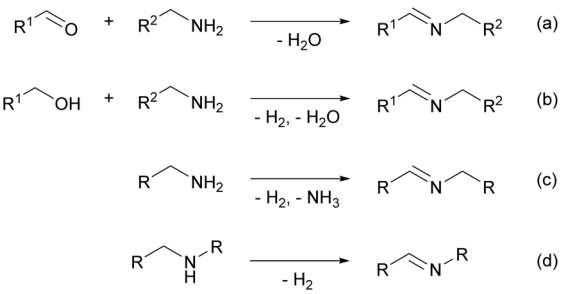

Scheme 1 Different approaches to the synthesis of imines.

the synthesis of nitrogen heterocycles, fine chemicals and pharmacologically active compounds.[4] Although the condensation of carbonyl compounds and amines has been traditionally practiced for the synthesis of imines (Scheme 1a),[5] in recent years, there has been a general upsurge of interest in developing alternative approaches based on air or molecular oxygen as green terminal oxidants,[6] namely: (a) the oxidative cross dehydrogenation of alcohols and amines (Scheme 1b),[7] (b) the direct oxidation of primary amines (Scheme 1c),[8] and (c) the oxidative dehydrogenation of secondary amines (Scheme 1d).[8,9] The combination of aerobic methods with photochemical conditions offers an operating surplus with respect to conventional protocols in terms of efficiency, atom economy and sustainability.[10]

Within the cyclic amines, 3,4-dihydroisoquinolines are worth mentioning because of their potential application in medicinal chemistry. For instance, ancistrocladidine is a natural naphthyl-dihydroisoquinoline alkaloid isolated from the plant family Ancistrocladaceae, the extracts of which have been used in traditional medicine to treat malaria and dysentery (Chart 1).[11] There is an ongoing interest in the synthesis of 1,2,3,4-tetrahydroisoquinolines because they are considered privileged structures in drug discovery, with diverse therapeutic applications.[12] In this sense, the C=N bond of 3,4-dihydroisoquinolines can be conveniently exploited to obtain substituted 1,2,3,4-tetrahydroisoquinolines through manifold organic reactions;[13] solifenacin (Vesicare™) is one of these types of compounds, a muscarinic receptor antagonist effective against overactive bladder disorders (Chart 1).[14] While the oxidative dehydrogenation of 1,2,3,4-tetrahydroisoquinolines seems a straightforward access to 3,4-dihydroisoquinolines,[9] this approach is hampered because of the trend to over-oxidation of the latter, leading to the corresponding aromatic isoquinolines.[15] In particular, 3,4-dihydroisoquinoline can be

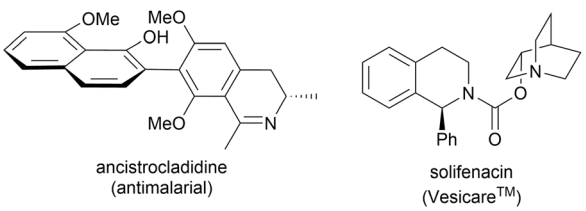

Chart 1 The structures of the biologically active dihydroisoquinoline ancistrocladidine and the tetrahydroisoquinoline solifenacin.

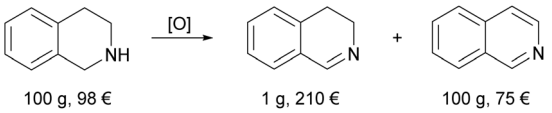

Scheme 2 Products of the oxidative dehydrogenation of 1,2,3,4-tetrahydroisoquinoline and prices (Sigma-Aldrich, 2026).

considered a high-value chemical, the price of which is much higher than that of 1,2,3,4-tetrahydroisoquinoline and isoquinoline (Scheme 2).

Since the recent revival of interest in photocatalysis,[16] different research groups have used this kind of activation to attempt the challenging transformation of 1,2,3,4-tetrahydroisoquinoline (THIQ) into 3,4-dihydroisoquinoline (DHIQ), typically, using O_2 as a terminal oxidant. A variety of catalytic systems has been tested, including those based on (a) ruthenium complexes,[17] (b) organic dyes,[18] (c) porphyrins,[19] (d) polymers,[20] (e) MOFs,[21] and carbon nitride,[22] among others.[23] Although, generally, moderate-to-high selectivity is attained in the title transformation with the aforementioned photocatalysts, most of them are relatively expensive and/or involve laborious synthetic procedures. Within heterogeneous photocatalysis, titania[24] is a simple, cheap, stable, non-toxic and very important semiconductor photocatalyst employed in organic chemistry transformations.[25] Titania (anatase) was found to promote the dehydrogenation of THIQ with 100% conversion and 68% selectivity under visible-light irradiation at 40 °C.[26] It is known that metal doping can improve the photocatalytic activity of TiO_2 by tuning the bandgap and regulating its electronic properties.[27] The metal dopant can behave as an electron trap, improving the transfer, migration and separation of electrons and holes; it can also shift the bandgap absorption to visible light, furnishing a surface with additional active sites for photochemical reactions.[28] The modification of TiO_2 with transition metals, such as Pt, Ni and Rh, was explored for the semi-oxidation of THIQ; however, the conversions and/or selectivities towards DHIQ reported were relatively low.[29] Therefore, despite the notable advances in the field, many of the reported systems suffer from inherent limitations in photocatalytic efficiency and/or sustainability. These include modest conversions or selectivities, the need for complex and costly catalysts, and procedures that lack alignment with green chemistry principles.

We are experienced in using TiO_2 as a support for metal nanoparticles,[30] as well as a heterogeneous photocatalyst[31] in varied organic reactions. Our particular ongoing interest in developing efficient catalysts based on copper nanoparticles (CuNPs), led to the recent discovery of sulfur-stabilised CuNPs promoting the mild oxidation of primary amines to imines, using the molecular oxygen in air as a terminal oxidant.[32] Also recently, we demonstrated that a glass-wool based molybdenum disulfide-cobalt semiconductor catalyst (MoCo@GW) could catalyse the semi-oxidation of THIQ through a singlet oxygen path, reaching a conversion and selectivity of 90%.[33] Given this recent interest in imine synthesis, together with the fact that nanocomposites can manifest enhanced photocatalytic

performance,[34] we have prepared a series of monometallic and bimetallic nanoparticle-supported titania-based photocatalysts, whose performance in the transformation of THIQ into DHIQ has been tested and compared with that of the metal-free counterparts. A thorough optimisation of the conditions has been carried out by using different variables such as atmosphere, solvent, base, catalyst amount, radiation wavelength, and power density. It is known that the efficient heterojunction formed at the interface of rutile and anatase polymorphs in TiO_2-P25,[35] along with the presence of oxidised Cu species that introduce additional energy levels near the valence and conduction bands of TiO_2,[36] contributes to a synergistic effect that can enhance photocatalytic activity. Based on these properties, we present a recyclable CuNPs/TiO_2-P25 catalytic system for the selective semi-oxidation of THIQ, which aligns with green chemistry and sustainability principles. Our current study not only achieves photocatalytic performance comparable to the best systems reported to date in terms of conversion and selectivity, but offers a more balanced sustainability profile, thus representing a significant advancement in the field of green photocatalysis.

Results and discussion

Preparation of the supported catalysts

The supported catalysts were prepared following a general chemical reduction method of metal salts previously reported by us.[37] In this method, the anhydrous metal salt (*e.g.*, $CuCl_2$) is reduced by metal lithium in the presence of a catalytic amount of 4,4′-di-*tert*-butylbiphenyl (DTBB), which acts as an electron carrier (Scheme 3). The rapid generation of the metal nanoparticles is followed by the addition of the TiO_2 support, filtration and drying. Handling of the catalysts from this point was done under air. The preparation of bimetallic catalysts supported on TiO_2 followed the same strategy as described in Scheme 3, but starting from an equimolar mixture of the metal salts.

Bandgap energy measurements

The bandgap energy (E_g) of the different catalysts was determined *via* Diffuse Reflectance Spectroscopy (DRS) with a suitable UV-vis spectrophotometer and ignoring specular reflection (see the SI). All the CuNPs-based photocatalysts experienced some decrease in the bandgap energy with respect to that of TiO_2-P25 (Degussa-Evonik unless otherwise stated), which was more pronounced in the case of CuNPs/TiO_2-P25 non-Degussa-Evonik) (Table 1, entries 1–5). A particle-size effect was observed when comparing the E_g of CuNPs/TiO_2 (anatase 15 nm) and CuNPs/TiO_2 (anatase 4 nm), with the latter being 0.23 eV lower (Table 1, entries 4 and 5). The monometallic catalyst based on MnNPs showed the same behaviour as that of CuNPs/TiO_2-P25 (Table 1, entries 2 and 6), whereas the bimetallic systems gave disparate results: the E_g slightly decreased for CuMnNPs/TiO_2-P25 and CuFeNPs/TiO_2-P25, but notably dropped for CuNiNPs/TiO_2-P25, with this being the lowest E_g recorded (Table 1, entries 7–9). Indeed, this value is considerably lower than those reported for the mixed oxides NiO/TiO_2 (2.81–2.99 eV) or for Ni- and S-doped TiO_2 (2.87 eV).[38]

Table 1 Bandgap energies determined for TiO_2-based catalysts

Entry	Catalyst[b]	λ (nm)	E_g (eV)
1	TiO_2-P25[a]	397	3.20
2	CuNPs/TiO_2-P25	441	2.88
3	CuNPs/TiO_2-P25[b]	460	2.76
4	CuNPs/TiO_2 (anatase 15 nm)	412	3.08
5	CuNPs/TiO_2 (anatase 4 nm)	445	2.85
6	MnNPs/TiO_2-P25	441	2.88
7	CuMnNPs/TiO_2-P25	400	3.17
8	CuNiNPs/TiO_2-P25	475	2.67
9	CuFeNPs/TiO_2-P25	420	3.02

[a] Degussa-Evonik TiO_2-P25, unless otherwise stated. [b] Non-Degussa-Evonik TiO_2-P25.

Photocatalytic experiments

Preliminary experiments for the selective oxidation of THIQ (**1**) to DHIQ (**2**) were conducted in MeCN using a near-UV irradiation (369 nm) at 0.14 W cm^{-2} power density for 3 h under an oxygen atmosphere, as the general conditions (Table 2). A control reaction in the absence of any catalyst led to unreacted THIQ (**1**), even after 23 h (Table 2, entry 1). Then, we focused on the photocatalytic activity of TiO_2-P25 (Degussa-Evonik). The effect of the atmosphere demonstrated the necessity for an oxidising medium, with molecular oxygen giving better results than air in terms of conversion after 3 h (Table 2, entries 2–4). It is noteworthy that quantitative conversion could be reached under air after 24 h, though the selectivity towards DHIQ (**2**) was lower than that with molecular oxygen (Table 2, compare entries 2 and 4). The catalyst loading and power density were also analysed as variables. The best results were obtained with 10 mg of TiO_2-P25 in MeCN (Table 2, compare entry 2 with entries 5–7) and a power density of 0.14 W cm^{-2} (Table 2, compare entry 2 with entries 8–14). Double amount of TiO_2-P25 did not affect the selectivity, but diminished the conversion at 3 h (Table 2, entry 7); quantitative conversion was reached with extended reaction time, albeit with no improvement in the selectivity (Table 2, entry 7). Power densities lower than 0.14 W cm^{-2} led to significant conversions only after 23 h (Table 2, entries 8–11), whereas higher power densities favoured the formation of **3** after 3 h and

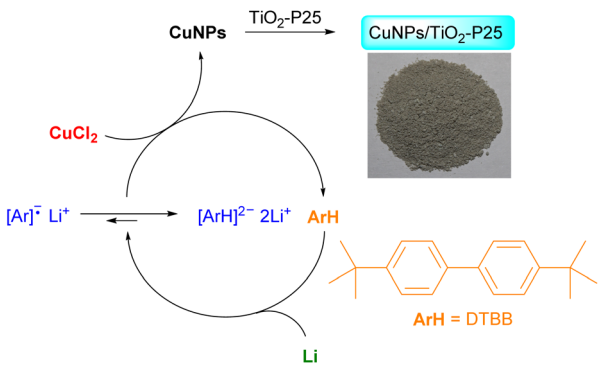

Scheme 3 Reaction scheme for the synthesis of CuNPs/TiO_2-P25.

Table 2 Photocatalysed oxidative dehydrogenation of THIQ (**1**): effect of the catalyst amount and power density in different atmospheres[a]

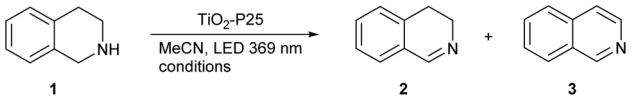

1 **2** **3**

Entry	Catalyst	Atmosphere	Catalyst amount (mg)	Power density (W cm^{-2})	Conversion[b] (%)	Selectivity **2**/**3** [b] (%)
1	—	O_2	—	0.14	0 (0)	—
2	**TiO_2-P25**	**O_2**	**10.0**	**0.14**	**97**	**84**
3	TiO_2-P25	Ar	10.0	0.14	0	0
4	TiO_2-P25	Air	10.0	0.14	75 (>99)	89 (70)
5	TiO_2-P25	O_2	1.7	0.14	78	78
6	TiO_2-P25	O_2	5.0	0.14	78	59
7	**TiO_2-P25**	**O_2**	**20.0**	**0.14**	**89 (>99)**[c]	**84 (84)**[c]
8	TiO_2-P25	O_2	10.0	0.005	0 (82)	(80)
9	TiO_2-P25	Air	10.0	0.005	0 (90)	(54)
10	TiO_2-P25	O_2	10.0	0.07	0 (82)	(80)
11	TiO_2-P25	Air	10.0	0.07	0 (79)	(77)
12	TiO_2-P25	O_2	10.0	0.20	44	25
13	TiO_2-P25	Air	10.0	0.20	25	40
14	TiO_2-P25	O_2	10.0	0.28	44	11
15	TiO_2-P25	O_2	10.0	—[d]	0 (8)	(88)
16	TiO_2-P25[e]	O_2	10.0	0.14	(26)	(15)

[a] Reaction conditions: **1** (0.5 mmol), TiO_2-P25 (Degussa-Evonik), MeCN (2 mL), LED 369 nm, O_2 (balloon) or air. [b] Conversion of **1** into **2** and **3** determined by GLC after 3 h (no by-products were observed); data after 23 h in parentheses. [c] Data after 16 h. [d] Reaction without irradiation. [e] Calcined at 500 °C for 4 h.

product decomposition after 23 h (Table 2, entries 12–14). A control experiment in the absence of irradiation led to only 8% conversion after 23 h, proving the very low catalytic effect by TiO_2-P25 itself (Table 2, entry 15). Although the photocatalytic activity of TiO_2-P25 has been reported to be enhanced after calcination[39] in the oxidation of methyl orange, we have not observed such effect in the oxidation of THIQ (**1**) (Table 2, entry 16).

The effect of the atmosphere was studied in more detail by monitoring the evolution of the oxidative dehydrogenation of THIQ (**1**) in oxygen (Fig. S2). The selectivity to DHIQ (**2**) peaked after 2 h (87%) at 89% conversion. Conversion then increased to a nearly quantitative value after 3 h (97%), while selectivity decreased to 84%. Prolonged irradiation promoted further oxidation of DHIQ (**2**) to IQ (**3**), with the latter being the major product after 23 h.

The effect of the solvent polarity and base were evaluated next, with the results being summarized in Table 3. A decrease in the conversion was noticed when water was introduced in the reaction medium as a mixture of MeCN-H_2O, while maintaining the selectivity observed with neat MeCN (compare entry 2 in Table 2 with entries 1 and 2 in Table 3).

The conversion decrease was more pronounced when using neat water as a solvent, particularly, in air (Table 3, entries 3 and 4). In these cases, quantitative conversions were reached after 23 h, though to the detriment of the selectivity (Table 3, entries 3 and 4). Within the organic solvents, isopropanol gave the best conversion at 3 h in oxygen with a good selectivity (Table 3, entry 5); this selectivity was maintained in air but with much lower conversion (Table 3, entry 6). Toluene and chloroform led to good-to-high conversions in air only after 23 h, with moderate selectivities (Table 3, entries 11 and 13). The effect of the presence of 1 equiv. of base on the reaction rate was also considered after 3 h in air, using neat water as a solvent (Table 3, entries 15–21): good-to-high selectivities were generally recorded, with Cs_2CO_3 showing the best performance (Table 3, entry 19). The favourable effect of Cs_2CO_3 was also observed in organic solvents, leading to the highest conversions and selectivities in air after 3 h (Table 3, entries 22–24). Among the organic solvents tested, MeCN afforded the most favourable outcome (92% conversion and 92% selectivity, 3 h in air), reaching quantitative conversion after 23 h with only a slight decrease in selectivity (Table 3, entry 22). When the catalyst loading was doubled to 20 mg, conversion remained high (91%), although the selectivity decreased to 82%.

We next examined the effect of the metal in the form of nanoparticles supported on TiO_2 (Table 4). Two wavelengths were selected to test the photocatalytic activity of the different prepared catalysts in the oxidative dehydrogenation of THIQ (**1**): near-UV light (λ = 369 nm) and blue visible light (λ = 450–455 nm). First, several catalysts based on CuNPs supported on different types of TiO_2 were screened under oxygen and 369 nm irradiation for 3 h at 0.14 W cm^{-2} power density (Table 4, entries 1–5). It is noteworthy that the type of TiO_2 used exerted an important influence in both the conversion and selectivity. For instance, CuNPs on 4 nm TiO_2 showed better performance than the 15 nm counterpart (Table 4, entries 4 and 5). The highest conversion at 3 h (90%) was attained with CuNPs/TiO_2-P25 (Table 4, entry 1), with 91% selectivity towards DHIQ (**2**). Notably, upon increasing the catalyst loading to 20 mg and

Table 3 Photocatalysed oxidative dehydrogenation of THIQ (**1**): effect of the solvent and base in oxygen and air[a]

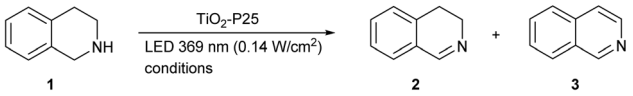

Entry	Solvent	Base	Atmosphere	Conversion[b] (%)	Selectivity **2**/**3** [b] (%)
1	MeCN-H_2O[c]	—	O_2	77	87
2	MeCN-H_2O[c]	—	Air	68	87
3	H_2O	—	O_2	64 (>99)	77 (66)
4	H_2O	—	Air	39 (>99)	77 (70)
5	*i*-PrOH	—	O_2	88	85
6	*i*-PrOH	—	Air	40	85
7	MeOH	—	O_2	39	49
8	DMSO	—	O_2	81	77
9	DMSO	—	Air	22	60
10	Toluene	—	O_2	65	91
11	Toluene	—	Air	0 (94)	(70)
12	$CHCl_3$	—	O_2	70	80
13	$CHCl_3$	—	Air	0 (81)	(78)
14	THF	—	O_2	61	67
15	H_2O	KOH	Air	29	83
16	H_2O	K_3PO_4	Air	29	83
17	H_2O	$NaHCO_3$	Air	53	89
18	H_2O	K_2CO_3	Air	20	85
19	H_2O	Cs_2CO_3	Air	60	90
20	H_2O	$Ba(OH)_2 \cdot 8H_2O$	Air	12	75
21	H_2O	KO*t*-Bu	Air	52	88
22	**MeCN**	**Cs_2CO_3**	**Air**	**92 (>99) [91]**	**92 (88) [82]**
23	DMSO	Cs_2CO_3	Air	82	94
24	*i*-PrOH	Cs_2CO_3	Air	87	92

[a] Reaction conditions: **1** (0.5 mmol), TiO_2-P25 (Degussa-Evonik, 10 mg), base (1 equiv.), solvent (2 mL), LED 369 nm (0.14 W cm^{-2}), O_2 (balloon) or air. [b] Conversion of **1** into **2** and **3** determined by GLC after 3 h; data after 23 h in parentheses; data with 20 mg of catalyst after 16 h in brackets. [c] 1 : 1 MeCN-H_2O.

extending the irradiation time, both conversion and selectivity approached quantitative values (97%). An important decrease in the conversion was observed when the above experiment at 3 h was conducted with CuNPs on calcined TiO_2-P25, albeit both conversion and selectivity reached high values after 23 h (Table 4, entry 2). Catalysts based on metals other than Cu led to lower conversions and selectivities (Table 4, entries 6–9), though MnNPs/TiO_2-P25 manifested quite good behaviour in this transformation (Table 4, entry 6). The reaction catalysed by CuNPs/TiO_2-P25 was also attempted under visible light irradiation (blue LED, λ = 450–455 nm) and in the absence of irradiation, in both cases producing minute amounts of the desired product after 23 h (Table 4, entries 10 and 11, respectively). The addition of Cs_2CO_3 did not improve the conversion and maintained the selectivity, but longer reaction time was needed (Table 4, entry 12). Reactions carried out in air were much less efficient regarding the conversion, irrespective of the solvent or base used (Table 4, entries 14–19).

In analogy to TiO_2-P25, the effect of reaction time was examined in more detail by monitoring the evolution of the oxidative dehydrogenation of THIQ (**1**) under an oxygen atmosphere using CuNPs/TiO_2-P25 (Fig. S3). The reaction profile shows a rapid consumption of the substrate and formation of DHIQ (**2**), reaching 90% conversion after 3 h with 91% selectivity. Importantly, after this initial period the product distribution becomes essentially time-independent: DHIQ (**2**) remains the dominant product while only minor amounts of IQ (**3**) are formed, and no progressive shift towards **3** is observed upon prolonged irradiation. In contrast to TiO_2-P25 (Fig. S2), where prolonged irradiation promotes further oxidation of DHIQ (**2**) to IQ (**3**) and, therefore, leads to a pronounced time-dependence of selectivity, the CuNPs/TiO_2-P25 system reaches a quasi-stationary regime within a few hours. As a result, selectivity is far less sensitive to extended reaction times, which is advantageous for reaction screening and substrate scope studies, as a single, standard irradiation time can be used without risking substantial over-oxidation.

The experimental results collected in Tables 2, 3, and 4 highlight the influence of several key variables on the conversion and selectivity of the oxidative dehydrogenation of THIQ (**1**): (a) the amount of photocatalyst shows a non-linear correlation with performance: while insufficient catalyst leads to incomplete conversion, a larger amount can promote light scattering and reduce the effective photon absorption, thus limiting photocatalytic efficiency and conversion at short reaction times; at longer reaction times, however, both conversion and selectivity improved further, particularly in the case of CuNPs/TiO_2-P25. (b) The nature of the atmosphere also plays a significant role: oxygen

Table 4 Photocatalysed oxidative dehydrogenation of THIQ (**1**): effect of the supported metal[a]

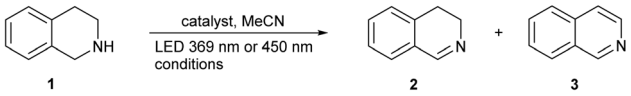

1 **2** **3**

Entry	Catalyst	Atmosphere-solvent-base	λ (nm)	Power density (W cm^{-2})	Conversion[b] (%)	Selectivity **2**/**3** [b] (%)
1	**CuNPs/TiO_2-P25**	**O_2**	**369**	**0.14**	**90 [97]**	**91 [97]**
2	CuNPs/TiO_2-P25[c]	O_2	369	0.14	41 (89)	96 (94)
3	CuNPs/TiO_2-P25[d]	O_2	369	0.14	60	88
4	CuNPs/TiO_2 (anatase 4 nm)	O_2	369	0.14	80	89
5	CuNPs/TiO_2 (anatase 15 nm)	O_2	369	0.14	65	86
6	MnNPs/TiO_2-P25	O_2	369	0.14	84	85
7	CuMnNPs/TiO_2-P25	O_2	369	0.14	35	91
8	CuNiNPs/TiO_2-P25	O_2	369	0.14	23	87
9	CuFeNPs/TiO_2-P25	O_2	369	0.14	23	91
10	CuNPs/TiO_2-P25	O_2	450–455	—	0 (16)	0 (13)
11	CuNPs/TiO_2-P25	O_2	—[e]	—[e]	0 (11)	0 (91)
12	CuNPs/TiO_2-P25	O_2-Cs_2CO_3	369	0.14	(81)	(90)
13	CuNPs/TiO_2-P25	Air	369	0.14	53	96
14	CuNPs/TiO_2-P25	Air-H_2O	369	0.14	28	93
15	CuNPs/TiO_2-P25	Air-MeCN/H_2O	369	0.14	47	94
16	CuNPs/TiO_2-P25	Air-*i*-PrOH	369	0.14	23	91
17	CuNPs/TiO_2-P25	Air-$NaHCO_3$	369	0.14	23	83
18	CuNPs/TiO_2-P25	Air-Cs_2CO_3	369	0.14	15	80
19	CuNPs/TiO_2-P25	Air-KO*t*-Bu	369	0.14	10	60

[a] Reaction conditions: **1** (0.5 mmol), catalyst (10 mg), MeCN (2 mL), LED 369 nm (0.14 W cm^{-2}) or 450–455 nm (18 W), unless otherwise stated, O_2 (balloon) or air; TiO_2-P25 refers to Degussa-Evonik material. [b] Conversion of **1** into **2** and **3** determined by GLC after 3 h; data after 23 h in parentheses; data with 20 mg of catalyst after 16 h in brackets. [c] With TiO_2-P25 calcined at 500 °C for 4 h. [d] Non-Degussa-Evonik TiO_2-P25. [e] Reaction without irradiation.

provides a higher concentration of reactive oxygen species (*e.g.*, singlet oxygen, superoxide radical anion), which facilitates rapid substrate oxidation, albeit can lead to overoxidation; air can slow down this process, enabling better selectivity for DHIQ (**2**) but at extended times. (c) Power density is another critical factor: lower irradiance slows down the generation of electron–hole pairs and reactive species, limiting conversion, while excessive power density can accelerate side reactions, compromising both conversion and selectivity. (d) Regarding the solvent effect, polar aprotic solvents like MeCN and DMSO provide the best results, likely due to their ability to dissolve polar intermediates and/or stabilise charged transition states. In contrast, protic or non-polar solvents often reduce activity, either by competing for reactive sites (*e.g.*, water, some alcohols–except *i*-PrOH) or by limiting the dispersion of the catalyst and substrate. (e) The addition of bases can improve the selectivity and, in some cases, the conversion; Cs_2CO_3 in particular might better promote the deprotonation of intermediates and facilitate product release from the surface, while also stabilising charged species, possibly minimising overoxidation. (f) As regards the nature of the metal supported on TiO_2, CuNPs outperform other transition metal nanoparticles, probably due to the favourable band alignment of Cu_2O with TiO_2, promoting effective charge separation and efficient generation of reactive oxygen species. The structural and electronic synergy can be further enhanced in CuNPs/TiO_2-P25, which combines the mixed-phase anatase/rutile interface (facilitating electron–hole separation) with the p–n heterojunction formed between TiO_2 and Cu_2O. (g) Additionally, the particle size and surface properties of the TiO_2 support modulate performance: smaller nanoparticles and the P25 formulation offer a higher surface area and more accessible active sites, as well as beneficial light-harvesting properties.

In summary, the data in Tables 2–4 show that the conversion-selectivity balance in the oxidative dehydrogenation of THIQ (**1**) depends strongly on the photocatalyst, the reaction atmosphere, and the irradiation time. Under an oxygen atmosphere, TiO_2-P25 enables rapid attainment of high conversion, with a moderate decrease in selectivity as conversion increases. In contrast, in air, the TiO_2-P25/Cs_2CO_3 system provides a favourable compromise between conversion and selectivity without the need for pure oxygen. Finally, CuNPs/TiO_2-P25 under oxygen combines high selectivity with high conversion and, under extended irradiation at higher catalyst loading, approaches near-quantitative values for both parameters.

Given the particularly high performance of CuNPs/TiO_2-P25 among the supported photocatalysts, and considering its combination of high conversion and selectivity under oxygen, a detailed characterisation of this material was undertaken to gain further insight into its structural and electronic features.

Characterisation of CuNPs/TiO_2-P25

The catalyst CuNPs/TiO_2-P25 was characterised by different analytical and spectroscopic techniques, such as ICP-OES, EDX, XRD, XPS, FE-SEM and TEM. The copper loading on

CuNPs/TiO_2-P25 was determined to be 3.0 wt%, as analysed by Inductively-Coupled Plasma-Optical Emission Spectroscopy (ICP-OES). The obtained adsorption isotherm (N_2 at 77 K) shows that CuNPs/TiO_2-P25 is a material with low adsorption capacity (Fig. 1). The isotherm can be classified as a type III, typical of macroporous or non-porous materials, where the adsorbent–adsorbate interactions are relatively weak. The type-H3 hysteresis loop is usually linked with the non-rigid nature of the adsorbent.[40] In agreement with the low adsorption capacity of CuNPs/TiO_2-P25, the calculated BET(N_2) (Brunauer–Emmett–Teller) surface area is 50.3 $m^2\ g^{-1}$, which is within some of the ranges reported for TiO_2-P25 alone,[41] but lower than that determined by us for TiO_2-P25 alone (82.0 $m^2\ g^{-1}$). A pore volume of 0.998 $cm^3\ g^{-1}$ has been estimated by applying the BJH model to the desorption branch data, with an average size of 2.7 nm.[40] Energy-Dispersive X-ray (EDX) analysis on various regions confirmed the presence of copper on TiO_2, with energy bands of 8.04, 8.90 keV (K lines) and 0.93 keV (L line) (Fig. 2); the presence of carbon is due to the use of a carbon support during the analysis. The estimated superficial atomic distribution by EDX gives a 3.2 wt% Cu, close to the copper content determined by ICP-OES. The examination of CuNPs/TiO_2-P25 by powder X-ray diffraction (XRD) (Fig. 3) showed diffraction peaks mainly corresponding to anatase and rutile; no significant peak for copper was observed due to the small crystal domains, low copper loading and/or high dispersion. Similarly, the Raman spectrum mainly shows the characteristic peaks of TiO_2-P25 at 146, 198, 398, 518 and 639 cm^{-1}.[42] Peaks corresponding to Cu_2O (201, 300, 406, 489 and 638 cm^{-1}) and CuO (274, 328 and 627 cm^{-1})[43] are of low intensity and/or with shifts very close to those of TiO_2-P25 (Fig. 4). Nevertheless, it is known that both XRD and Raman techniques have low sensitivity towards Cu_2O, particularly, when the copper loading is low.[44]

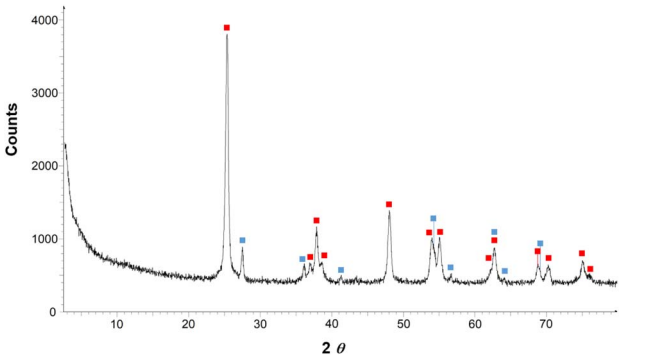

Fig. 3 XRD spectrum of CuNPs/TiO_2-P25 (■ TiO_2 anatase; ■ TiO_2 rutile).

The oxidation state of copper was studied by X-ray Photoelectron Spectroscopy (XPS) at the Cu $2p_{3/2}$ level (Fig. 5). The peaks at 932.1 (Cu^I) and 933.6 (Cu^{II}) eV, together with the satellite peaks at 940.5 and 943.1 eV, which are a typical feature of Cu^{II} species,[45] suggest that the catalyst is mainly composed of Cu_2O and a minor amount of CuO. According to our previous experience,[30c,d] the presence of some superficial Cu^0 can be practically disregarded as the catalyst has been handled in air. Auger spectroscopy on

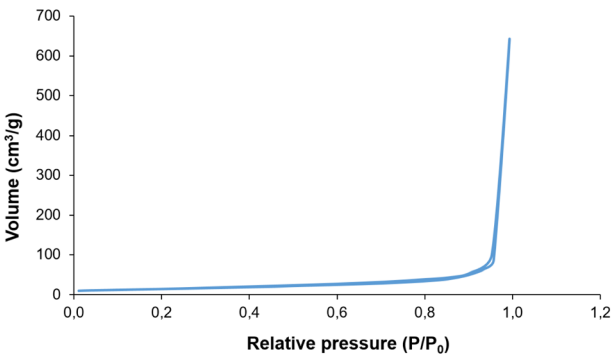

Fig. 1 Adsorption nitrogen isotherm on CuNPs/TiO_2-P25.

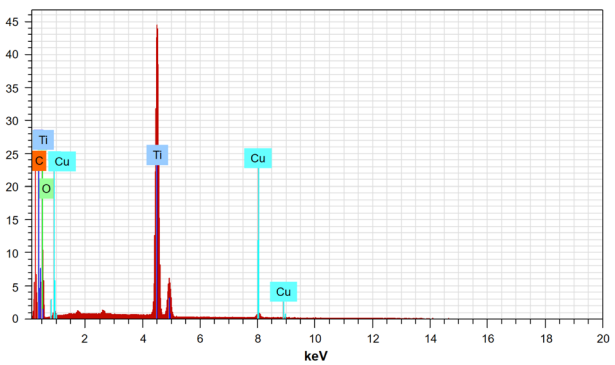

Fig. 2 EDX spectrum of CuNPs/TiO_2-P25.

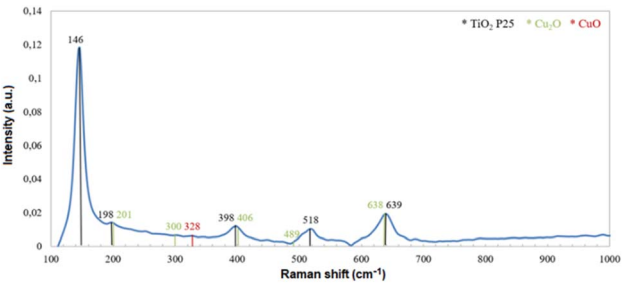

Fig. 4 Raman spectrum of CuNPs/TiO_2-P25.

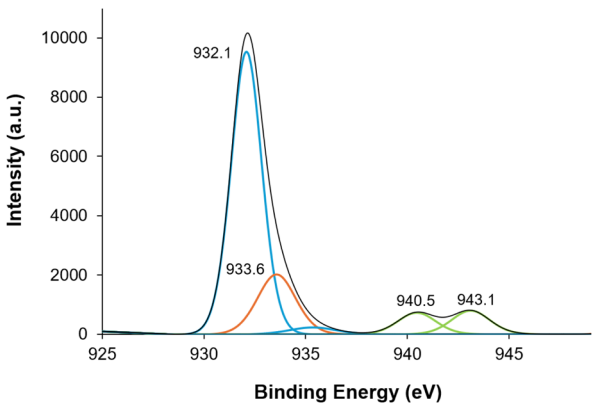

Fig. 5 XPS spectrum at the Cu $2p_{3/2}$ level of CuNPs/TiO_2-P25.

CuNPs/TiO_2-P25 (Cu LMM lines) was inconclusive in this case because the 2 s transition of Ti interferes with that of Cu, being the former much stronger and making the latter difficult to interpret.

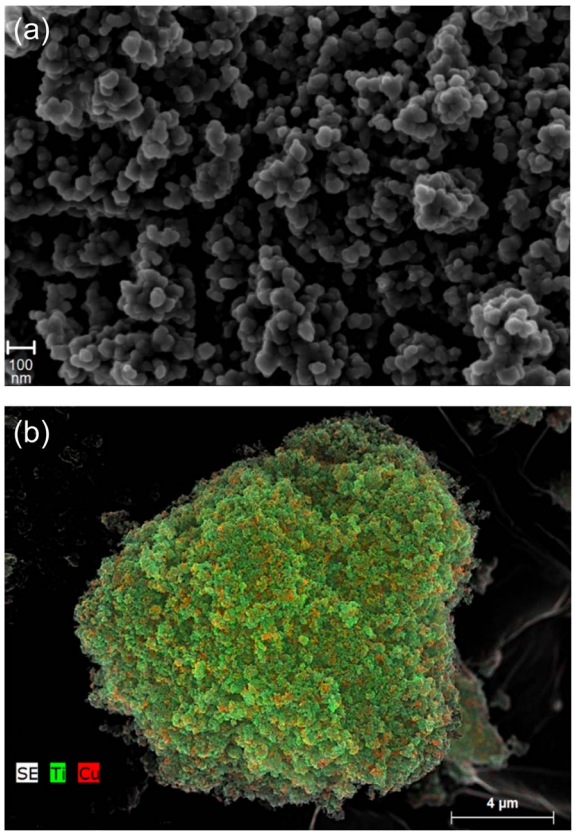

Fig. 6 (a) FE-SEM micrograph and (b) EDS elemental mapping of CuNPs/TiO_2-P25.

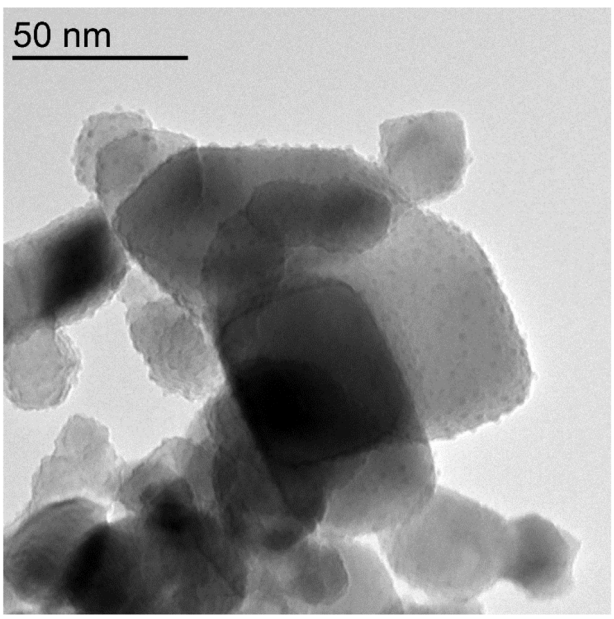

Fig. 7 HR-TEM micrograph of CuNPs/TiO_2-P25.

The morphology of the catalyst was examined by FE-SEM (Field Emission Scanning Electron Microscopy), with the EDS (Energy Dispersive Spectroscopy) elemental mapping showing a homogeneous distribution of Cu over the TiO_2 surface (Fig. 6). HR-TEM (High Resolution Transmission Electron Microscopy) further revealed discrete, well-dispersed particles decorating the support (mostly in the range 2–3 nm), which could be assigned to Cu-based nanoparticles (Fig. 7).

Having established the composition and morphology of CuNPs/TiO_2-P25, we next explored the catalytic performance across a broader range of substrates.

Substrate scope

Rather than aiming at an extensive exploration of the substrate scope, this study was designed primarily to compare the catalytic behaviour of TiO_2-P25 and CuNPs/TiO_2-P25. The system TiO_2-P25-Cs_2CO_3 (air), although also efficient, was not included in this comparative study in order to simplify the catalytic conditions and focus the analysis on the intrinsic effect of copper on titania. To this end, a representative panel of amines was examined under our standard conditions (Chart 2). As a baseline, the oxidation of 1,2,3,4-tetrahydroisoquinoline (THIQ) to dihydroisoquinoline (**2**) reveals very similar behaviour for both photocatalysts, indicating that this particularly activated benzylic substrate is efficiently transformed even in the absence of copper. This similarity extends to another unfunctionalised THIQ precursor leading to product **5**, whereas a clear divergence emerges for the methoxy-substituted THIQ that furnishes product **4**: in this case, CuNPs/TiO_2-P25 delivers a substantially higher efficiency than bare TiO_2-P25. A closely

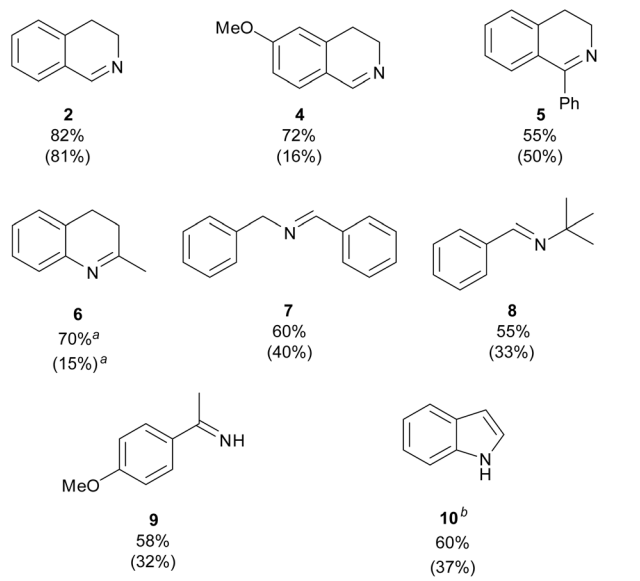

Chart 2 Photocatalysed oxidative dehydrogenation of various amines using CuNPs/TiO_2-P25 and TiO_2-P25: amine (0.5 mmol), CuNPs/TiO_2-P25 or TiO_2-P25 (10 mg), MeCN (2 mL), LED 369 nm (0.14 W cm^{-2}), O_2 (balloon), 24 h. Yields of the isolated products[46] are reported for CuNPs/TiO_2-P25; yields obtained with TiO_2-P25 are shown in parentheses. [a]Conversion to compound **6** determined by GLC. [b]Product obtained from indoline.

related scaffold, 2-methyltetrahydroquinoline (precursor of **6**), further exemplifies the different behaviour of the two materials, with CuNPs/TiO_2-P25 clearly outperforming TiO_2-P25 in this case. The same qualitative picture holds for the two acyclic secondary amines (precursors of **7** and **8**): CuNPs/TiO_2-P25 consistently affords substantially higher yields than TiO_2-P25. For the benzylic primary amine (precursor of **9**), the reaction delivers the primary imine selectively; notably, no secondary imine arising from self-condensation of two primary amine units was detected under our conditions. Once again, CuNPs/TiO_2-P25 shows a clear efficiency advantage over TiO_2-P25. Finally, the transformation of indoline to indole (**10**) is less informative from a selectivity standpoint but remains a useful activity probe: CuNPs/TiO_2-P25 achieves a distinctly higher level of dehydrogenation than TiO_2-P25, in line with the broader trend observed for the more challenging substrates above. Overall, the general enhanced performance of CuNPs/TiO_2-P25 might be attributed to a more efficient copper-assisted interfacial electron transfer.

Catalyst reuse

We examined the reusability of the most active photocatalysts under the optimised conditions. Preliminary attempts to reuse the three best catalytic systems identified above—TiO_2-P25 in O_2 (Table 2, entry 2), TiO_2-P25-Cs_2CO_3 in air (Table 3, entry 22) and CuNPs/TiO_2-P25 in O_2 (Table 4, entry 1)—were carried out under the standard conditions (10 mg of catalyst, 3 h) over three consecutive cycles, with catalyst recovery by centrifugation and drying in air. Under these conditions, TiO_2-P25 in O_2 displayed a pronounced loss of activity, with conversion decreasing from 95% to 50% over the three cycles, while the selectivity remained approximately constant (*ca.* 82%) (Table S1, entry 1). Likewise, TiO_2-P25-Cs_2CO_3 in air showed a progressive decrease in conversion (92% to 48%) accompanied by a moderate erosion in selectivity (91% to 80%) (Table S1, entry 2). In contrast, CuNPs/TiO_2-P25 in O_2 maintained essentially unchanged performance over the three cycles (90–91% conversion and 91–93% selectivity), indicating a markedly more stable catalytic behaviour under the standard conditions (Table S1, entry 3).

To gain insight into the origin of the activity loss observed for TiO_2-P25 upon reuse, we recorded XPS spectra of the photocatalyst recovered after the third cycle under the standard conditions (10 mg, 3 h) (Fig. S5a). Comparison with reference materials obtained by impregnation of TiO_2-P25 with THIQ (**1**), DHIQ (**2**) and IQ (**3**) indicates that the N 1s region of the recycled catalyst is more consistent with that of TiO_2-P25/DHIQ (**2**) (Fig. S7a), whereas the spectra of TiO_2-P25/THIQ (**1**) and TiO_2-P25/IQ (**3**) are markedly different. Although a definitive assignment is not possible based on the N 1s signal alone, these data are consistent with the presence of adsorbed DHIQ (**2**) or DHIQ-derived nitrogen-containing species on the TiO_2-P25 surface after recycling. Such adsorption/passivation could reduce the number of accessible active sites and thereby contribute to the decrease in conversion upon reuse, while having a comparatively limited impact on selectivity.

To compensate for small handling losses between cycles, recycling experiments were subsequently performed with 20 mg of catalyst (extended irradiation, 16 h). The three best catalytic systems above were tested, with the copper-modified material showing the most robust performance (Tables 5, S1 and Fig. S4). Thus, CuNPs/TiO_2-P25 converted THIQ (**1**) almost quantitatively over the first four cycles with sustained high selectivity to DHIQ (**2**) (conversions 97–96%, **2**/**3** 97:3–96:4) (Table 5, entry 3; Fig. 8 and S4c); only a drop in conversion was observed in the fifth run (75%, the corresponding lactam was detected), though maintaining high **2**/**3** selectivity (95%). In contrast, TiO_2-P25 (O_2) and TiO_2-P25–Cs_2CO_3 (air) displayed progressive losses of activity (99–85% and 91–70%, respectively) and, more markedly, of selectivity (84:16–39:61 and 82:18–50:50, respectively), over three cycles (Table 5, entries 1 and 2; Table S1, Fig. S4a and b). These trends are consistent with the time-dependent over-oxidation observed for TiO_2-P25 under O_2, whereby DHIQ (**2**) is progressively converted into IQ (**3**) upon prolonged irradiation. Together with the XPS evidence suggesting retention of DHIQ-derived species on recycled TiO_2-P25, this is compatible

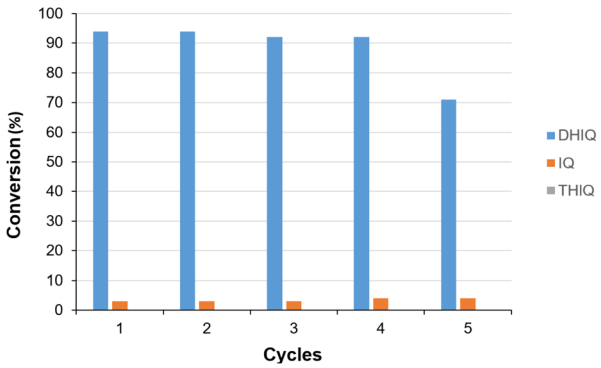

Fig. 8 Reuse of CuNPs/TiO_2-P25 in the photocatalysed oxidative dehydrogenation of THIQ (**1**): **1** (0.5 mmol), CuNPs/TiO_2-P25 (20 mg), MeCN (2 mL), LED 369 nm (0.14 W cm^{-2}), in O_2 (balloon). The conversion of THIQ (**1**) into DHIQ (**2**) and IQ (**3**) was determined by GLC after 16 h.

Table 5 Reuse of the three best photocatalysts in the oxidative dehydrogenation of THIQ (**1**)[a]

Entry	Catalyst	Base-atmosphere	Conversion[b] (%)	Selectivity **2**/**3** [b] (%)
1	TiO_2-P25	O_2	>99, 95, 85	84, 79, 39
2	TiO_2-P25	Cs_2CO_3-air	91, 88, 70	82, 77, 50
3	CuNPs/TiO_2-P25	O_2	97, 97, 95, 96, 75	97, 97, 97, 96, 95

[a] Reaction conditions: **1** (0.5 mmol), catalyst (20 mg), base (1 equiv.), MeCN (2 mL), LED 369 nm (0.14 W cm^{-2}). [b] Conversions of THIQ (**1**) into DHIQ (**2**) and IQ (**3**), and selectivities for 3–5 consecutive cycles were determined by GLC after 16 h.

with partial surface passivation and a diminished ability to preserve chemoselectivity upon reuse, in contrast to the more stable behaviour of CuNPs/TiO_2-P25.

Overall, although all three materials are recyclable, CuNPs/TiO_2-P25 best preserves both conversion and chemoselectivity upon reuse, showing consistent behaviour under both standard (10 mg, 3 h) and extended (20 mg, 16 h) conditions.

A series of experiments, in the presence and absence of THIQ (**1**), were conducted to assess the potential copper leaching in CuNPs/TiO_2-P25 (Scheme 4). Practically no leaching was detected under dark conditions (Scheme 4a and c), and only a very small amount of copper (0.006%) was released upon irradiation in the absence of the substrate (Scheme 4d). A higher value (0.10%) was measured when both THIQ (**1**) and light were present, which we ascribe to substrate-CuNPs interactions under photoexcitation (Scheme 4b). The minor extraction observed under catalytic conditions might contribute to the decrease in performance observed after the fifth reuse cycle (Fig. 8).

We also explored the possibility of nitrogen species remaining attached to the photocatalyst surface upon reuse. In this respect, XPS analysis at the N 1s level of CuNPs/TiO_2-P25 after the first (397.8, 399.5 and 401.4 eV) and fifth (398.1, 399.7 and 401.4 eV) runs shows peaks in close proximity (Fig. S5). These peaks are similar to those recorded for TiO_2-P25 (399.4 and 401.2 eV) and CuNPs/TiO_2-P25 (398.5 and 399.8 eV) impregnated with DHIQ (**2**) (Fig. S7). Therefore, the Cu leaching observed, together with a partial passivation of the surface by nitrogen species (mainly DHIQ), might account for the decrease in catalytic activity observed after four cycles.

Acetonitrile has been ranked in different studies as a problematic solvent, within a scale of recommended, problematic, hazardous and highly hazardous solvents.[47] Although a small amount of MeCN was used in the experiments (2 mL), we demonstrated that 80% of the pure solvent could be easily recovered by microdistillation. Taking into account the mass of waste generated in five runs (5 × 0.4 mL MeCN + 20 mg CuNPs/TiO_2), and the mass of product in five reaction crudes (306 mg), an *E*-factor of 5.2 was obtained for the first four cycles. Although the *E*-factor was originally conceived for the chemical industry, it can also be applied at the laboratory scale as a metric of overall reaction performance. The calculated *E*-factor is satisfactory, since an ideal value should approach 0.[48]

Reaction mechanism

The differences in activity and selectivity observed between TiO_2-P25 and CuNPs/TiO_2-P25 prompted a series of mechanistic experiments to gain further insight into their catalytic behaviour. First, any possible interaction between TiO_2-P25 and the starting THIQ (**1**) was assessed. For this purpose, TiO_2-P25 was impregnated with THIQ (**1**) and analysed by Diffuse Reflectance Spectroscopy (DRS). The F(R) *vs.* the wavelength function of the impregnated TiO_2-P25 was shifted to higher wavelength than that of TiO_2-P25, into the visible region of the spectrum (Fig. S9). The bandgap energy (λ = 502 nm, E_g = 2.53 eV) is smaller than those of TiO_2 and CuNPs/TiO_2-P25 (E_g = 2.88 eV). Due to the dissociative character of the N–H bond in amines, they might associate with the TiO_2 surface, facilitating their oxidation *via* single-electron transfer and generating an electron charge-transfer complex. This type of interaction was previously reported by some of us in the case of TiO_2 impregnated with indole.[49]

Attenuated Total Reflectance Fourier-Transform Infrared Spectroscopy (ATR-FTIR) experiments were also conducted on THIQ, TiO_2-P25 and THIQ/TiO_2-P25. The region around 3300 cm^{-1} shows the practical disappearance of the signals related to the NH bond of THIQ (**1**) (compare the red and purple lines, Fig. 9) and the broad OH signal of TiO_2-P25 (compare the orange and purple lines, Fig. 9). The peak around 1650 cm^{-1}, attributable to the N–H bond bending of THIQ, has experienced a notable decrease in THIQ/TiO_2-P25. These results support an interaction between the NH bond of THIQ (**1**) and the OH groups on the TiO_2-P25 surface, and point to THIQ (**1**) being attached to the surface of TiO_2-P25.

The presence of CuNPs on TiO_2-P25 altered the surface of the latter and its interaction with the substrate, which was assessed by XPS. Analysis of the XPS spectra of THIQ/TiO_2-P25 and THIQ/CuNPs/TiO_2-P25 at the N 1s level showed a pronounced shift to higher binding energy for one of the THIQ peaks, from 401.1 to 406.9 eV, respectively (Fig. 10 and S6). These results are consistent with an enhanced interaction between THIQ (**1**) and the surface in CuNPs/TiO_2-P25. Interestingly, when both TiO_2-P25 and CuNPs/TiO_2-P25 were impregnated with DHIQ (**2**), the opposite trend was observed: the aforementioned band remained at essentially the same binding energy in TiO_2-P25 (401.2 eV), but decreased in CuNPs/TiO_2-P25 (398.6 eV), shifting below that in TiO_2-P25. The weaker interaction between DHIQ

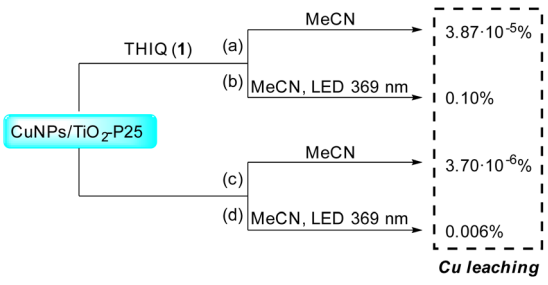

Scheme 4 Cu leaching in CuNPs/TiO_2-P25 under different conditions. All experiments were conducted under an O_2 atmosphere for 23 h.

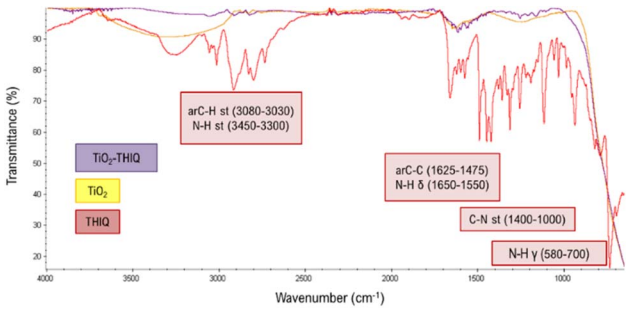

Fig. 9 ATR-FTIR spectra of THIQ (**1**), TiO_2-P25 and TiO_2-P25 impregnated with **1**.

(2) and CuNPs/TiO_2-P25 could facilitate desorption of the product from the surface, limiting its further oxidation to IQ and resulting in higher selectivity. This view is supported by the XPS data obtained after recycling TiO_2-P25, which are in line with retention of DHIQ-derived species on the surface (stronger interaction) and may contribute to catalyst passivation and, under extended reaction conditions, to a reduced ability to preserve chemoselectivity.

We also explored the effect of different scavengers in the oxidation of THIQ (**1**) photocatalysed by TiO_2-P25 and CuNPs/TiO_2-P25 (Table 6). The addition of NaN_3 and β-carotene, which are $^1O_2$ scavengers, substantially decreased the conversion, suggesting the participation of singlet oxygen both under TiO_2-P25 or CuNPs/TiO_2-P25 catalysis (entries 1–4). A similar depleting effect was noticed after the addition of *p*-quinone, a superoxide anion-radical scavenger, supporting an essential role of $O_2^{\cdot -}$ species in the process (entries 5 and 6). In contrast, the presence of *i*-PrOH as a $HO^{\cdot}$ scavenger did not alter so much the conversion, especially, in the case of TiO_2-P25 (entry 7); in the case of CuNPs/TiO_2-P25, we must take into account that isopropanol can be oxidised to acetone, competing with THIQ (**1**) as a substrate, a side reaction that could be enhanced in the presence of CuNPs and which could alter the properties of the latter (entry 8). Nevertheless, both results point to the fact that the hydroxy radical is not formed in large amount or is not crucial in the reaction. The role of $AgNO_3$ as an electron scavenger was less reliable in this reaction because of its capacity to directly oxidise the substrate (entries 9 and 10); in fact, IQ (**3**) was the major product formed when 3 equiv. of $AgNO_3$ were added (entries 9 and 10, footnote d). The addition of Et_3N, a hole scavenger, totally inhibited the reaction both with TiO_2-P25 and with CuNPs/TiO_2-P25 (entries 11 and 12). The selectivity was not much affected by the presence of the scavengers, with the exception of $AgNO_3$, being in most cases >85%.

Table 6 Photocatalysed oxidative dehydrogenation of THIQ (**1**) in the presence of different scavengers[a]

Entry	Catalyst[b]	Additive	Conversion[c] (%)	Selectivity **2**/**3** [c] (%)
1	TiO_2	NaN_3	35	86
2	CuNPs/TiO_2	NaN_3	16	81
3	TiO_2	β-carotene	33	88
4	CuNPs/TiO_2	β-carotene	23	61
5	TiO_2	*p*-quinone	14	86
6	CuNPs/TiO_2	*p*-quinone	20	80
7	TiO_2	*i*-PrOH	88	85
8	CuNPs/TiO_2	*i*-PrOH	57	89
9	TiO_2	$AgNO_3$	49 (78)[d]	89 (<0.01)[d]
10	CuNPs/TiO_2	$AgNO_3$	71 (80)[d]	91 (<0.01)[d]
11	TiO_2	Et_3N[d]	0	—
12	CuNPs/TiO_2	Et_3N[d]	0	—

[a] **1** (0.5 mmol), catalyst (10 mg), scavenger (1.2 equiv.), MeCN (2 mL), LED 369 nm (0.14 W cm^{-2}), O_2 (balloon), 23 h. [b] TiO_2-P25 (Degussa-Evonik). [c] Conversion of **1** into **2** and **3** determined by GLC. [d] 3.0 equiv. of the additive.

The analytical iodometry method was applied to the standard reactions under O_2 catalysed by TiO_2-P25 and CuNPs/TiO_2-P25: KI was added to both reactions showing a colour change from pale yellow in THIQ (**1**) to brown shades, typical of the I_3^- species formed upon oxidation of I^- by H_2O_2 (Fig. 11a). The *in situ* formation of H_2O_2 was additionally confirmed by using test strips specific for peroxide detection (Fig. 11b). The fact that the colour observed was lighter brown in the case of CuNPs/TiO_2-P25 could be due to this catalyst partially decomposing H_2O_2 through a Fenton-like reaction.[50]

Light-dark experiments were conducted under the standard conditions with the catalyst of choice for the title reaction: CuNPs/TiO_2-P25 (Fig. 12). The progress of the reaction depicted supports that constant irradiation is necessary for the process being productive, something that correlates with quite short or absence of radical-chain events.[51] The small increase in the conversion observed during the dark periods of time might be due to a background reaction involving the action of only CuNPs. This secondary catalytic activity, albeit of low magnitude, cannot be ruled out, as we previously described the oxidation of primary amines to imines catalysed by Cu_2ONPs/S_8.[32]

TiO_2 is a n-type semiconductor, with bandgaps of 3.2 eV (anatase) and 3.0 eV (rutile). TiO_2-P25 is a 75/25 mixture of anatase and rutile phases, which electron-acceptor character of the latter favours electron (e^-) and hole (h^+) separation, hampering their recombination.[35b] In contrast, Cu_2O is a common p-type semiconductor with a narrower bandgap of approximately 2.2 eV. When combined with TiO_2, they can form a p–n heterojunction. This heterojunction, which has been

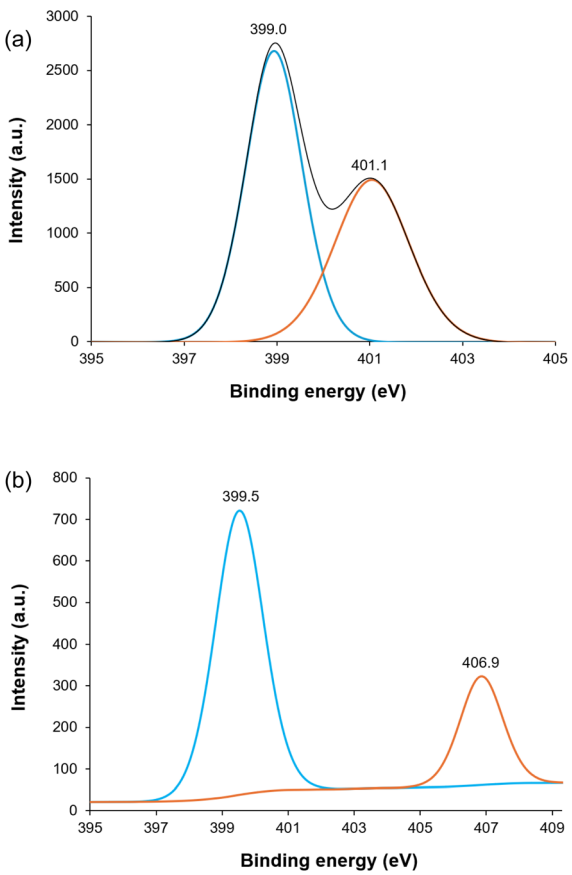

Fig. 10 XPS spectra at the N 1s level of (a) TiO_2-P25 and (b) CuNPs/TiO_2-P25, both impregnated with THIQ (**1**).

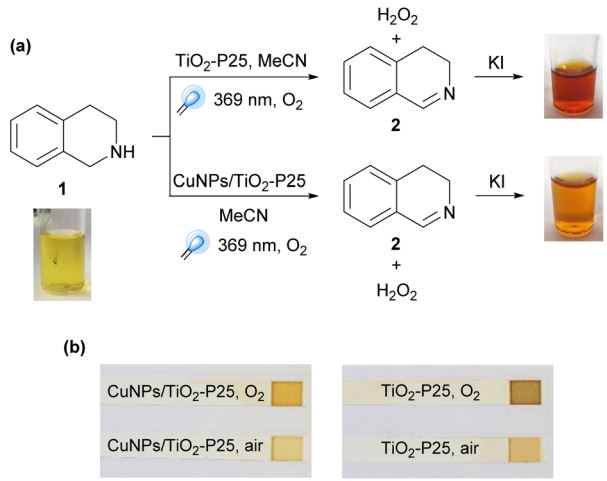

Fig. 11 (a) Iodometric detection of H_2O_2 in the transformation of **1** into **2** photocatalysed by TiO_2-P25 and CuNPs/TiO_2-P25. (b) Peroxide test applied to the same reactions in O_2 and air.

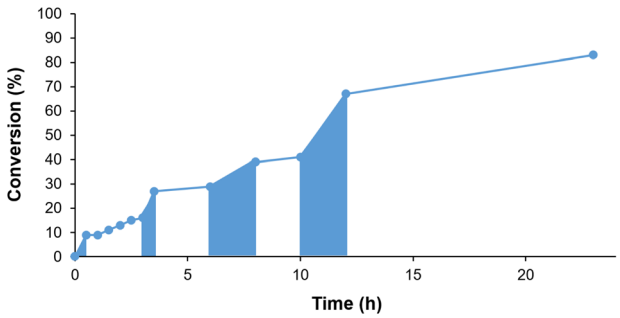

Fig. 12 Light-dark experiments in the transformation of **1** into **2** photocatalysed by CuNPs/TiO_2-P25. The blue areas correspond to light irradiation.

studied in detail by the group of Marotta for photocatalytic hydrogen production,[52] has two key benefits: it can decrease the bandgap energy, absorbing solar radiation more effectively and it can enhance the separation of the photogenerated charge carriers, leading to improved photocatalytic efficiency.

Taking into account the above studies and the results obtained, a reaction mechanism has been proposed (Scheme 5); only the anatase form of TiO_2 is represented to simplify the drawing and avoid uncertainty in the band alignments between rutile and anatase.[35] First, it is expected that both Cu_2O and TiO_2 are excited under the near-UV light irradiation. Then, electrons can migrate from the CB of Cu_2O to that of TiO_2, and holes can migrate from the VB of TiO_2 to that of Cu_2O.[53] These charge-carrier transfers are thermodynamically favoured because both the VB and CB of TiO_2 are low-lying with respect to those of Cu_2O. The fact that in our case the Cu_2O particles in CuNPs/TiO_2-P25 are small, can make their contact surface with the TiO_2 particles larger, with a concomitant increase of the lifetime of the excited electrons and holes, resulting in higher quantum efficiency.[54] Given that the photocatalyst CuNPs/TiO_2-P25 is primarily composed of TiO_2 (97.0 wt%), electron transfer to molecular oxygen is expected to mostly occur from the CB of TiO_2, generating the superoxide radical anion ($O_2^{\bullet-}$). THIQ (**1**) would undergo SET to the holes at the VB of TiO_2 to form the corresponding radical cation; this event is perfectly plausible to occur simultaneously at the VB of Cu_2O, considering the above demonstrated and accentuated interaction between THIQ (**1**) and the catalyst in the presence of CuNPs. Hydrogen-atom abstraction from the THIQ radical cation by $O_2^{\bullet-}$ would form the THIQ iminium ion and hydroperoxide anion (HO_2^-), which would react each other to produce DHIQ (**2**) by deprotonation and hydrogen peroxide as a by-product.

Comparison with other catalysts

Finally, the photocatalytic activity of CuNPs/TiO_2-P25 in the oxidation of THIQ (**1**) to DHIQ (**2**) was compared with that of previously reported photocatalytic systems (Table S2). Yields of DHIQ (**2**) >97% were reported for rather sophisticated catalysts, such as a porphyrinic Zr-MOF (entry 1), a tetraphenylporphyrin (entry 2), a porous *N*-carbazolyl-9-fluorenone polymer (entry 6),

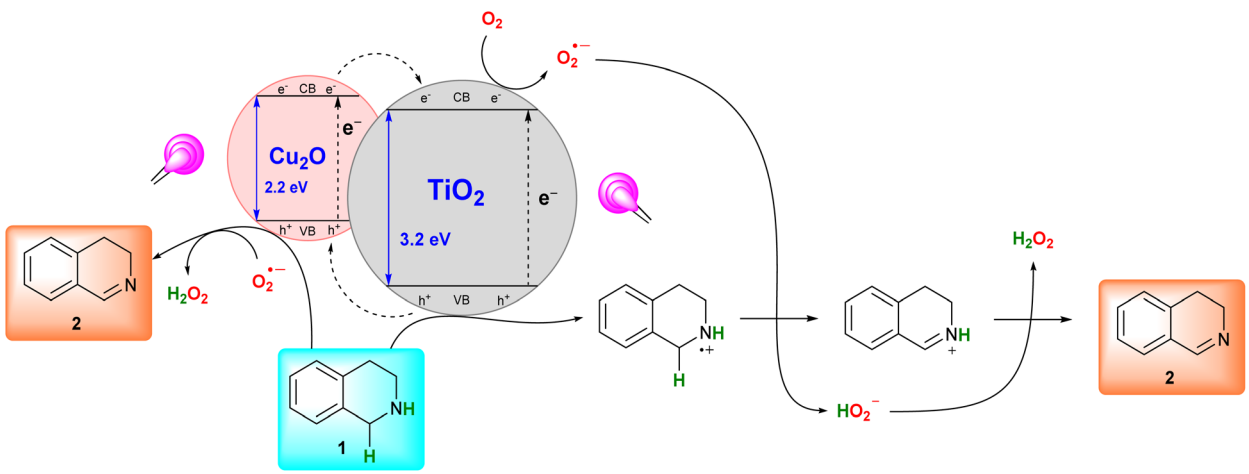

Scheme 5 Reaction mechanism proposed for the oxidative dehydrogenation of THIQ (**1**) to DHIQ (**2**) photocatalysed by CuNPs/TiO_2-P25. Only the anatase phase of TiO_2-P25 is shown for clarity.

and C_{70} (entry 8), typically using powerful lamps and, in the case of C_{70}, with chloroform as a solvent. Good conversions/yields and selectivities around 90% were attained with a Zn(II) chlorin complex (entry 4), a chromophore-cobaloxime (entry 5), CO_2-eosin Y (entry 9), mpg-C_3N_4 (entry 11), $Bi_2O_2CO_3$ (entry 13), Nb_2O_5 (entry 17), and $MoS_2/ZnIn_2S_4$ (entry 18). Some of these catalytic systems involve a rigorous inert atmosphere (entries 5 and 18), CO_2 instead of aerobic conditions (entry 9), pressure (entries 11 and 13), or benzene as a solvent (entry 17). Within the titania-based catalytic systems, neither TiO_2 anatase nor different metal-supported (Pt, Ni and Rh) titania photocatalysts were efficient, giving modest yields and/or selectivities (entries 19–22). In our hands, TiO_2-P25 under O_2 delivered quantitative conversion after extended irradiation, although the selectivity to DHIQ (**2**) remained moderate (entry 23). In contrast, CuNPs/TiO_2-P25 afforded substantially higher selectivity towards DHIQ (**2**) (97%), while maintaining excellent conversion (entry 24).

In order to better assess the advantages of a new method with respect to those previously published, it is highly recommended to examine their potential impact from the green chemistry point of view.[55] For that purpose, a series of factors were considered in both the photocatalytic procedures and in the preparation of the best-performing photocatalysts (Tables S3 and S4, respectively). In regard to the photocatalytic process, bio-accumulation, ecotoxicity, energy usage, global warming, eutrophication, flammability, human carcinogenicity, persistence, water consumption and the *E*-factor were analysed. Apparently, only the CO_2-eosin Y photocatalytic system can contribute to the bio-accumulation risk factor; eosin Y has a high potential to bio-concentrate and it would likely be mobile in the environment (*e.g.*, water systems) because of its water solubility (Table S3, entry 6, bio-accumulation column). Fortunately, all methods, with the exception of that involving Nb_2O_5 as photocatalyst, are free from ecotoxic issues; in this case, benzene is used as solvent, which is considered a highly toxic chemical to aquatic life, even at relatively low concentrations (Table S3, entry 9, ecotoxicity column). The catalysts we studied are composed of titania or copper and titania; copper is toxic to fish and Daphnia,[56] whereas titania is classified as a non-hazardous substance.[57] However, the amount of copper in the catalyst is small (3.0 wt%), and it is quite stabilised on the surface of the support which, in addition, is insoluble in water. Furthermore, we found out that CuNPs/TiO_2 increased ovarian cells viability;[30d] therefore, we can conclude that the potential ecotoxicity of this catalyst is negligible in any case (Table S3, entry 12). The comparison of energy usage among the photocatalytic procedures (Table S3) reveals three distinct categories: low-efficiency systems with relatively high energy consumption (>1 kWh, entries 2, 8, and 9), intermediate systems with moderate consumption (>0.3 and <1 kWh, entries 1, 3–7, and 10), and high-efficiency systems with low energy demand (<0.3 kWh, entries 11 and 12). Notably, the TiO_2-P25 and CuNPs/TiO_2-P25 systems exhibit the lowest energy consumption among all evaluated procedures (0.048 kWh, entries 11 and 12), highlighting their excellent energy efficiency and alignment with the principles of green chemistry. Only the method using C_{70} as photocatalyst might have a contribution to the global warming factor, because chloroform is utilised as solvent in the photocatalytic reaction and in the reaction work-up (Table S3, entry 5, global-warming column); although its direct warming effect may be limited, chloroform can contribute to global warming indirectly (*e.g.*, by ozone depletion). Nitrogenated compounds have a medium-risk contribution to eutrophication, which is decreased if they are volatile; six of the photocatalytic procedures involve non-volatile nitrogen-containing compounds (Table S3, entries 1–4, 6 and 7; eutrophication column). The flammability risk factor can be object of concern when compounds have flash points close or below the operating temperature; in this sense, mpg-C_3N_4 is applied at 80 °C in MeCN, with the latter having a flash point of 6 °C (Table S3, entry 7, flammability column). THF, chloroform and benzene are suspect of causing cancer; THF is used as a solvent in the chromophore-cobaloxime photocatalytic experiment, whereas chloroform and benzene are used not only in the photocatalytic experiments but in the work-up and reuse of C_{70} and Nb_2O_5 (Table S3, entries 3, 5 and 9, respectively; human-carcinogenicity column). Compounds with high molecular weight (*e.g.*, polymers) are persistent, and are involved in four procedures (Table S3, entries 1, 3, 4 and 7; persistence column). Water is consumed as co-solvent in one method and in the work-up of two methods; nonetheless, the amount of water used in the experiments is relatively small (Table S3, entries 6, 8 and 10; water-consumption column). Finally, the *E*-factor has been estimated taking into account the amount of catalyst, solvent, additives and the amount of product; unfortunately, the work-up has been excluded from the calculation because the amount of water or solvents used was not specified in all the procedures. The lowest *E*-factors were obtained for the protocols with tetraphenylporphyrin, Nb_2O_5, TiO_2-P25, and CuNPs/TiO_2-P25 (Table S3, entries 2, 9, 11 and 12, respectively; *E*-factor column).

Concerning the preparation of the photocatalysts, five are commercially available: tetraphenylporphyrin, C_{70}, eosin Y, Nb_2O_5 and the TiO_2-P25 (this work) (Table S4, entries 2, 5, 6, 9, and 11); among these, with the exception of Nb_2O_5 and TiO_2-P25, the remaining materials are relatively expensive (see footnotes *i*, *l* − *n*). The other photocatalysts were laboratory-made and, though all the procedures involve some risk factors, they are free from bio-accumulation and persistence concerns. Although six methods use water-soluble substances, which can be classified as ecotoxic, in four of them these substances are moderately soluble in water and are used in small amounts (Table S4, entries 7, 8, 10 and 12; ecotoxicity column); only in the preparation of porphyrinic Zr-MOF and chromophore-cobaloxime, highly water-miscible and ecotoxic DMF is used as solvent in relatively large amounts (Table S4, entries 1 and 3; ecotoxicity column). Five methods have an important contribution to the energy-usage factor, because they require prolonged heating at different temperatures, in one case in combination with high-power lamp irradiation (Table S4, entries 1, 3, 4, 7 and 10; energy-usage column); in contrast, the preparation of $Bi_2O_2CO_3$ and CuNPs/TiO_2-P25 takes place at room temperature, with the former needing mild warming in the drying step (Table S4, entries 8 and 12; energy-usage

column). All procedures, excluding that for CuNPs/TiO_2-P25 (Table S4, entry 12, eutrophication column), have a medium-risk contribution to eutrophication, because they involve nitrogen-containing compounds. Fortunately, the flammability risk factor is underrepresented, only affecting porphyrinic Zr-MOF, in which the starting material pyrrole has a flash point (36 °C) much lower than the operating temperature (140 °C) (Table S4, entry 1, flammability column). All protocols, excluding that for $Bi_2O_2CO_3$ (Table S4, entry 8, human carcinogenicity column) use some cancer suspect agents, while only those for the porous organic polymer and CuNPs/TiO_2-P25 are free from water consumption (Table S4, entries 4 and 12; water-consumption column). Another important aspect to take into account when preparing a catalyst is the number of synthetic steps, understood as those leading to a different compound, as well as the number of operations, such as filtration, washing, drying, extraction, *etc.* In general, straightforward procedures lead to lower amounts of waste, being more attractive and more probable to be implemented by other research groups. In this regard, CuNPs/TiO_2-P25, $Bi_2O_2CO_3$ and mpg-C_3N_4 were prepared in one step with two, three and four operations, respectively (Table S4, entries 7, 8 and 12; synthetic-steps column); the rest of the photocatalysts required 2–4 synthetic steps and 4–12 operations (Table S4, entries 1, 3, 4 and 10; synthetic-steps column). Finally, it is generally accepted that catalyst recycling is crucial to move towards a more sustainable and resource-efficient chemical production, with the heterogeneous catalysts being advantageous compared to the homogeneous counterparts because of the higher stability and easier separation from the reaction medium of the former. Tetraphenylporphyrin, the chromophore-cobaloxime and eosin Y photocatalysts were not reused at all (Table S4, entries 2, 3 and 6; catalyst-reuse column). The recycling capability of the rest of the photocatalysts is not easy to compare because some of them were reused in the oxidation of benzylamines (porphyrinic Zr-MOF, mpg-C_3N_4 and Nb_2O_5) or thioanisole (porous organic polymer) to the corresponding imines or sulfoxide, respectively (Table S4, entries 1, 4, 7 and 9; catalyst-reuse column); these substrates are less prone to over-oxidation than THIQ (**1**). C_{70}, $Bi_2O_2CO_3$, $MoS_2/ZnIn_2S_4$ and CuNPs/TiO_2-P25 were efficiently reused in the oxidation of THIQ (**1**) to DHIQ (**2**), showing a good performance in 3–5 cycles (Table S4, entries 5, 8, 10 and 12; catalyst-reuse column).

The information described above in Tables S3 and S4 has been condensed in Table 7. Tetraphenylporphyrin and C_{70} are among the photocatalysts with the lowest number of risk factors (entries 2 and 5); however, the risk factors associated with their preparation were not considered here because they are commercially available, albeit at high cost. In addition, tetraphenylporphyrin cannot be reused, and C_{70} requires carcinogenic chloroform in the photocatalytic reaction, leading to an *E*-factor >100. TiO_2-P25 (this work, entry 11) displays the most favourable hazard profile ($RF_t = 0$) together with a low *E*-factor (<30); nevertheless, its reuse was not efficient due to a marked loss of selectivity. Although the use of THF remains a drawback in the preparation of CuNPs/TiO_2-P25 (this work, entry 12), it can be replaced by greener alternatives such as 2-methylTHF.[47]

Table 7 Comparison of the efficiency and sustainability of the photocatalysts[a]

Entry	Photocatalyst	RF_{pr}	RF_{pp}	RF_t	E_{pr}	R
1	Porphyrinic Zr-MOF	2	6	8	>100	Y
2	Tetraphenylporphyrin	2	n/a	2	<30	N
3	Chromophore-cobaloxime	3	5	8	>100	N
4	Porous organic polymer	2	3	5	60–100	Y
5	C_{70}	2	n/a	2	>100	Y
6	CO_2, eosin Y	3	n/a	3	>100	N
7	mpg-C_3N_4	3	4	7	60–100	Y
8	$Bi_2O_2CO_3$	2	2	4	60–100	Y
9	Nb_2O_5	3	n/a	3	<30	Y
10	$MoS_2/ZnIn_2S_4$	1	4	5	>100	Y
11[b]	TiO_2-P25	0	n/a	0	<30	[c]
12[b]	CuNPs/TiO_2-P25	0	1	1	<10	Y

[a] For detailed information, see Tables S3 and S4. RF_{pr}: number of risk factors in the photocatalytic reaction. RF_{pp}: number of risk factors in the photocatalyst preparation. RF_t: total number of risk factors. E_{pr}: *E*-factor range in the photocatalytic reaction. R: catalyst reusability; Y (yes), N (no). [b] This work. [c] Catalyst reuse was not efficient because of the important loss of selectivity.

Overall, when risk factors, waste generation and recyclability are considered together, CuNPs/TiO_2-P25 provides the most balanced profile among the twelve photocatalytic systems evaluated.

Conclusions

The challenging transformation of 1,2,3,4-tetrahydroisoquinoline (THIQ) into 3,4-dihydroisoquinoline (DHIQ) has been thoroughly studied under heterogeneous photocatalytic conditions using a range of titania-based photocatalysts and oxygen as a terminal oxidant. Among them, TiO_2-P25 (O_2), TiO_2-P25-Cs_2CO_3 (air), and CuNPs/TiO_2-P25 (O_2) in acetonitrile can be regarded as the most efficient systems in terms of conversion and selectivity. While TiO_2-P25 (O_2) and TiO_2-P25-Cs_2CO_3 (air) offer simple and metal-free protocols achieving high conversions and good selectivities under mild aerobic conditions, CuNPs/TiO_2-P25 (mainly composed of Cu_2O nanoparticles on TiO_2-P25) displayed the most robust behaviour upon reuse, maintaining high conversions (97–96%) and selectivities (97:3–96:4) over the first four cycles. We have demonstrated that minor copper leaching occurs under the combined action of THIQ (**1**) and irradiation, which, together with partial surface passivation by nitrogen species, could account for the decline in activity observed from the fifth cycle onward. Moreover, CuNPs/TiO_2-P25 proved to be superior to TiO_2-P25 in the oxidative dehydrogenation of a variety of amines beyond THIQ, highlighting its broader applicability.

The application of different analytical techniques and mechanistic experiments supports that (a) there is a marked interaction between THIQ (**1**) and the surface of the photocatalysts, which is stronger in CuNPs/TiO_2-P25 than in TiO_2-P25; (b) the opposite trend observed for DHIQ (**2**) could be related to the higher selectivity recorded with CuNPs/TiO_2-P25, compared with TiO_2-P25; (c) $^1O_2$, $O_2^{\cdot-}$, h^+, and H_2O_2 species are

involved in the reaction; and (d) radical-chain processes are not predominant in this transformation. Accordingly, a reaction mechanism has been proposed.

In addition, the catalytic activity of CuNPs/TiO_2-P25 compares very favourably with that of most photocatalysts reported to date and stands at the level of the best-performing systems. A comprehensive analysis of sustainability-related factors in the catalyst preparation and photocatalytic procedures, including *E*-factor estimation and reusability, provides a more nuanced picture: while TiO_2-P25 exhibits the most favourable risk-factor score, its performance upon reuse is condition-dependent (a pronounced loss of conversion under standard conditions and a substantial loss of selectivity under extended conditions), whereas CuNPs/TiO_2-P25 offers a more balanced overall sustainability profile when risk factors, waste generation and catalyst reuse are considered together. Altogether, this work represents a meaningful advance over previous methodologies, combining high photocatalytic performance with operational simplicity, while highlighting how catalyst design can improve selectivity retention upon reuse in aerobic photocatalytic oxidations. These results may also open new avenues for research in heterogeneous photocatalysis applied to organic transformations, particularly those based on simple, inexpensive, stable and non-toxic titania.

Conflicts of interest

There are no conflicts to declare.

Data availability

The data supporting this article have been included as part of the supplementary information (SI). Supplementary information: general, procedures, E_g measurements, reaction profiles, DR and XPS spectra, tables, compound characterisation and NMR spectra. See DOI: https://doi.org/10.1039/d6su00169f.

Acknowledgements

This work was generously supported by the Generalitat Valenciana (GV, Spain; grants no. CIAICO/2022/017 and IDIFEDER/2021/013) and the Ministerio de Ciencia, Innovación y Universidades (MCIU, Spain; grant no. PID2024-155338NB-I00). I. M.-G. thanks the Vicerrectorado de Investigación of the Universidad de Alicante (Spain) for a pre-doctoral grant (no. UAFPU2016-034). P. R.-N. also thanks the Generalitat Valenciana (GV, Spain; grant no. CIACIF/2022/141) and the Ministerio de Ciencia, Innovación y Universidades (MCIU, Spain; grant no. FPU23/01445) for pre-doctoral grants.

Notes and references

1 General review: J. P. Adams, Imines, enamines and oximes, *J. Chem. Soc., Perkin Trans. 1*, 2000, **1**, 125–139.

2 Recent reviews: (*a*) J.-D. Yang, J. Xue and J.-P. Cheng, Understanding the role of thermodynamics in catalytic imine reductions, *Chem. Soc. Rev.*, 2019, **48**, 2913–2926; (*b*) R. Innocenti, E. Lenci and A. Trabocchi, Recent advances in copper-catalyzed imine-based multicomponent reactions, *Tetrahedron Lett.*, 2020, **61**, 152083; (*c*) K. Morisaki, H. Morimoto and T. Ohshima, Recent progress on catalytic addition reactions to N-unsubstituted imines, *ACS Catal.*, 2020, **10**, 6924–6951; (*d*) T.-C. Chang, A. R. Pradipta and K. Tanaka, Enantioselective synthesis of cyclic and linear diamines by imine cycloadditions, *Chirality*, 2020, **32**, 1160–1168; (*e*) S. A. Orr, P. C. Andrews and V. L. Blair, Main group metal-mediated transformations of imines, *Chem.–Eur. J.*, 2021, **27**, 2569–2588; (*f*) I. N. Egorov, S. Santra, G. V. Zyryanov, A. Majee, A. Hajra and O. N. Chupakhin, Direct asymmetric addition of heteroatom nucleophiles to imines, *Adv. Synth. Catal.*, 2022, **364**, 2092–2112.

3 Recent reviews: (*a*) N. F. Curtis, Syntheses and structures of compounds with acyclic imine ligands formed by reactions of coordinated amines with carbonyl compounds, *Inorg. Chim. Acta*, 2019, **498**, 118843; (*b*) S. Biswas, N. Patel, R. Deb and M. Majumdar, Chemistry of the bis(imine)-based tetradentate ligand stabilized group 14 E(II) cations (E=Ge and Sn), *Chem. Rec.*, 2022, **22**, e202200003; (*c*) C. Qian, L. Feng, W. L. Teo, J. Liu, W. Zhou, D. Wang and Y. Zhao, Imine and imine-derived linkages in two-dimensional covalent organic frameworks, *Nat. Rev. Chem.*, 2022, **6**, 881–898.

4 Reviews: (*a*) S. F. Martin, Recent applications of imines as key intermediates in the synthesis of alkaloids and novel nitrogen heterocycles, *Pure Appl. Chem.*, 2009, **81**, 195–204; (*b*) Y. Shan, L. Su, Z. Zhao and D. Chen, The construction of nitrogen-containing heterocycles from alkynyl imines, *Adv. Synth. Catal.*, 2021, **363**, 906–923.

5 (*a*) H. Schiff, Mittheilungen aus dem universitäts laboratorium in Pisa: eine neue reihe organischer basen, *Ann. Chem.*, 1864, **131**, 118–119; (*b*) L. J. Silverberg, D. J. Coyle, K. C. Cannon, R. J. Mathers, J. A. Richards and J. Thierney, Azeotropic preparation of a C-phenyl N-aryl imine: an introductory undergraduate organic chemistry laboratory experiment, *J. Chem. Educ.*, 2016, **93**, 941–944.

6 Review: Y. Yamamoto, S. Kodama, A. Nomoto and A. Ogawa, Innovative green oxidation of amines to imines under atmospheric oxygen, *Org. Biomol. Chem.*, 2022, **20**, 9503–9521.

7 Reviews: (*a*) S. Bähn, S. Imm, L. Neubert, M. Zhang, H. Neumann and M. Beller, The catalytic amination of alcohols, *ChemCatChem*, 2011, **3**, 1853–1864; (*b*) Y. Obora, Recent advances in α-alkylation reactions using alcohols with hydrogen borrowing methodologies, *ACS Catal.*, 2014, **4**, 3972–3981; (*c*) M. N. Kopylovich, A. P. Ribeiro, E. C. Alegria, N. M. Martins, L. M. Martins and A. J. Pombeiro, Catalytic oxidation of alcohols: Recent advances, *Adv. Organomet. Chem.*, 2015, **63**, 91–174.

8 Reviews: (*a*) M. Largeron, Protocols for the catalytic oxidation of primary amines to imines, *Eur. J. Org Chem.*, 2013, 5225–5235; (*b*) B. Chen, L. Wang and S. Gao, Recent advances in aerobic oxidation of alcohols and amines to imines, *ACS Catal.*, 2015, **5**, 5851–5876.

9 Review: S. Hati, U. Holzgrabe and S. Sen, Oxidative dehydrogenation of C–C and C–N bonds: A convenient approach to access diverse (dihydro)heteroaromatic compounds, *Beilstein J. Org. Chem.*, 2017, **13**, 1670–1692.

10 Review: X. Zhang, K. P. Rakesh, L. Ravindar and H.-L. Qin, Visible-light initiated aerobic oxidations: a critical review, *Green Chem.*, 2018, **20**, 4790–4833.

11 (*a*) T. R. Govindachari, P. C. Parthsarathy and H. K. Desai, Chemical investigation of Ancistrocladus heyneanus. Ancistrocladidine, a new isoquinoline alkaloid, *Indian J. Chem.*, 1973, **11**, 1190–1991; (*b*) M. A. Rizacassa, Total synthesis of naphthylisoquinoline alkaloids, *Nat. Prod. Chem.*, 1998, **20**, 407–455, and the references cited therein.

12 L. Yet. *Privileged Structures in Drug Discovery: Medicinal Chemistry and Synthesis*, John Wiley & Sons, Hoboken (NJ), 1st edn, 2018, pp. 356–413.

13 Review: (*a*) J. Iwanejko and E. Wojaczyńska, Cyclic imines – preparation and application in synthesis, *Org. Biomol. Chem.*, 2018, **16**, 7296–7314; (*b*) See also: L. Yang, J. Zhu, C. Sun, Z. Deng and X. Qu, Biosynthesis of plant tetrahydroisoquinoline alkaloids through an imine reductase route, *Chem. Sci.*, 2020, **11**, 364–371.

14 Review:D. Robinson and L. C. Solifenacin, pharmacology and clinical efficacy, *Expert Rev. Clin. Pharmacol.*, 2009, **3**, 239–253.

15 See, for instance: J.-J. Zhong, W.-P. To, Y. Liu, W. Lu and C.-M. Che, Efficient acceptorless photo-dehydrogenation of alcohols and N-heterocycles with binuclear platinum(II) diphosphite complexes, *Chem. Sci.*, 2019, **10**, 4883–4889.

16 Selected reviews: (*a*) Y. Lee and M. S. Kwon, Emerging organic photoredox catalysts for organic transformations, *Eur. J. Org Chem.*, 2020, 6028–6043; (*b*) W.-N. Cheng and R. Shang, Transition metal-catalyzed organic reactions under visible light: recent developments and future perspectives, *ACS Catal.*, 2020, **10**, 9170–9196; (*c*) S. Reischauer and B. Pieber, Emerging concepts in photocatalytic organic synthesis, *iScience*, 2021, **24**, 102209; (*d*) L. Candish, K. D. Collins, G. C. Cook, J. J. Douglas, A. Gómez-Suárez, A. Jolit and S. Keess, Photocatalysis in the life science industry, *Chem. Rev.*, 2022, **122**, 2907–2980.

17 (*a*) D. K. Tiwari, R. A. Maurya and J. B. Nanubolu, Visible-light/photoredox-mediated sp^3 C-H functionalization and coupling of secondary amines with vinyl azides in flow microreactors, *Chem.–Eur. J.*, 2016, **22**, 526–530; (*b*) F. Stanek, R. Pawlowski, P. Morawsk, R. Bujok and M. Stodulskiet, Dehydrogenation and α-functionalization of secondary amines by visible-light-mediated catalysis, *Org. Biomol. Chem.*, 2000, **18**, 2103–2112; (*c*) I. Echeverría, M. Vaquero, B. R. Manzano, F. A. Jalón and R. Quesada, *Inorg. Chem.*, 2022, **61**, 6193–6208.

18 (*a*) D. Riemer, W. Schilling, G. Goetz, Y. Zhang, S. Gehrke, I. Tkach, O. Hollóczki and S. Das, CO_2-catalyzed efficient dehydrogenation of amines with detailed mechanistic and kinetic studies, *ACS Catal.*, 2018, **8**, 11679–11687; (*b*) D. Chao and M. Zhao, A supramolecular assembly bearing an organic TADF chromophore: synthesis, characterization and light-driven cooperative acceptor less dehydrogenation of secondary amines, *Dalton Trans.*, 2019, **48**, 5444–5449.

19 (*a*) G. Jiang, J. Chen, J.-S. Huang and C. M. Che, Highly efficient oxidation of amines to imines by singlet oxygen and its application in Ugi type reactions, *Org. Lett.*, 2009, **11**, 4568–4571; (*b*) K. Marui, A. Nomoto, H. Akashi and A. Ogawa, Green oxidation of amines to imines based on the development of novel catalytic systems using molecular oxygen or hydrogen peroxide, *Synthesis*, 2016, **48**, 31–42; (*c*) J. Jin, C. Yang, B. Zhang and K. Deng, Selective oxidation of amines using O_2 catalyzed by cobalt thioporphyrazine under visible light, *J. Catal.*, 2018, **361**, 33–39.

20 (*a*) C. Su, R. Tandiana, B. Tian, A. Sengupta, W. Tang, J. Su and K. P. Loh, Visible-light photocatalysis of aerobic oxidation reactions using carbazolic conjugated microporous polymers, *ACS Catal.*, 2016, **6**, 3594–3599; (*b*) Y. Zhi, K. Li, H. Xia, M. Xue, Y. Mu and X. Liu, X. Robust porous organic polymers as efficient heterogeneous organo-photocatalysts for aerobic oxidation reactions, *J. Mater. Chem. A*, 2017, **5**, 8697–8704.

21 (*a*) C. Xu, H. Liu, D. Li, J.-H. Sub and H.-L. Jiang, Direct evidence of charge separation in a metal-organic framework: efficient and selective photocatalytic oxidative coupling of amines via charge and energy transfer, *Chem. Sci.*, 2018, **9**, 3152–3158; (*b*) Q. Han, Y.-L. Wang, M. Sun, C.-Y. Sun, S. S. Zhu, X.-L. Wang and Z.-M. Su, Metal-organic frameworks with organogold(III) complexes for photocatalytic amine oxidation with enhanced efficiency and selectivity, *Chem.–Eur. J.*, 2018, **24**, 15089–15095; (*c*) H. Li, Y. Yang, C. He, L. Zeng and C. Duan, Mixed-ligand metal-organic framework for two-photon responsive photocatalytic C-N and C-C coupling reactions, *ACS Catal.*, 2019, **9**, 422–430.

22 (*a*) F. Su, S. C. Mathew, L. Möhlmann, M. Antonietti, X. Wang and S. Blechert, Aerobic oxidative coupling of amines by carbon nitride photocatalysis with visible light, *Angew. Chem., Int. Ed.*, 2011, **50**, 657–660; (*b*) S. Juntrapirom, S. Anuchai, O. Thongsook, S. Pornsuwan, P. Meepowpan, P. Thavornyutikarn, S. Phanichphant, D. Tantraviwat and B. Inceesungvorn, Photocatalytic activity enhancement of g-C_3N_4/BiOBr in selective transformation of primary amines to imines and its reaction mechanism, *Chem. Eng. J.*, 2020, **394**, 124934.

23 (*a*) S. Furukawa, Y. Ohno, T. Shishido, K. Teramura and T. Tanaka, Selective amine oxidation using Nb_2O_5 photocatalyst and O_2, *ACS Catal.*, 2011, **1**, 1150–1153; (*b*) L. Huang, J. Zhao, S. Guo, C. Zhang and J. Ma, Bodipy derivatives as organic triplet photosensitizers for aerobic photoorganocatalytic oxidative coupling of amines and photooxidation of dihydroxylnaphthalenes, *J. Org. Chem.*, 2013, **78**, 5627–5637; (*c*) R. Kumar, E. H. Gleißner, E. G. V. Tiu and Y. Yamakoshi, C_{70} as a photocatalyst for oxidation of secondary benzylamines to imines, *Org. Lett.*, 2016, **18**, 184–187; (*d*) P. Bai, X. Tong, J. Wan, Y. Gao and S. Xue, Flower-like $Bi_2O_2CO_3$-mediated selective oxidative

coupling processes of amines under visible light irradiation, *J. Catal.*, 2019, **374**, 257–265.

24 Reviews: (*a*) J. Schneider, M. Matsuoka, M. Takeuchi, J. Zhang, Y. Horiuchi, M. Anpo and D. W. Bahnemann, Understanding TiO_2 photocatalysis: mechanisms and materials, *Chem. Rev.*, 2014, **114**, 9919–9986; (*b*) Q. Guo, Z. Ma, C. Zhou, Z. Ren and X. Yang, Single molecule photocatalysis on TiO_2 surfaces, *Chem. Rev.*, 2019, **119**, 11020–11041.

25 Reviews: (*a*) X. Lang, X. Chen and J. Zhao, Heterogeneous visible light photocatalysis for selective organic transformations, *Chem. Soc. Rev.*, 2014, **43**, 473–486; (*b*) D. W. Manley and J. C. Walton, Preparative semiconductor photoredox catalysis: An emerging theme in organic synthesis, *Beilstein J. Org. Chem.*, 2015, **11**, 1570–1582; (*c*) P. Riente and T. Noël, Application of metal oxide semiconductors in light-driven organic transformations, *Catal. Sci. Technol.*, 2019, **9**, 5186–5232; (*d*) S. Kohtani, A. Kawashima and H. Miyabe, Stereoselective organic reactions in heterogeneous semiconductor photocatalysis, *Front. Chem.*, 2019, **7**, 630; (*e*) J. C. Scaiano and A. E. Lanterna, A green road map for heterogeneous catalysis, *Pure Appl. Chem.*, 2020, **92**, 63–73.

26 X. Lang, W. Ma, Y. Zhao, C. Chen, H. Ji and J. Zhao, Visible-light-induced selective photocatalytic aerobic oxidation of amines into imines on TiO_2, *Chem.–Eur. J.*, 2012, **18**, 2624–2631.

27 Reviews: (*a*) H. Park, Y. Park, W. Kim and W. Choi, Surface modification of TiO_2 photocatalyst for environmental applications, *J. Photochem. Photobiol. C Photochem. Rev.*, 2013, **15**, 1–20; (*b*) H. Cheng and W. Xu, Recent advances in modified TiO_2 for photo-induced organic synthesis, *Org. Biomol. Chem.*, 2019, **17**, 9977–9989; (*c*) See, also, for instance: J. Dong, J. Ye, D. Ariyanti, Y. Wang, S. Wei and W. Gao, Enhancing photocatalytic activities of titanium dioxide via well dispersed copper nanoparticles, *Chemosphere*, 2018, **204**, 193–201.

28 Reviews: (*a*) V. Kumaravel, S. Mathew, J. Bartlett and S. C. Pillai, Photocatalytic hydrogen production using metal doped TiO_2: A review of recent advances, *Appl. Catal. B Environ.*, 2019, **244**, 1021–1064; (*b*) M. R. Al-Mamun, S. Kader, M. S. Islam and M. Z. H. Khan, Photocatalytic activity improvement and application of UV-TiO_2 photocatalysis in textile wastewater treatment: A review, *J. Environ. Eng.*, 2019, **7**, 103248.

29 (*a*) P. Bai, X. Tong, Y. Gao and P. Guo, Oxygen-free water-promoted selective photocatalytic oxidative coupling of amines, *Catal. Sci. Technol.*, 2019, **9**, 5803–5811; (*b*) N. O. Balayeva, N. Zheng, R. Dillert and D. W. Bahnemann, Visible-light mediated photocatalytic aerobic dehydrogenation of N-heterocycles by surface grafted TiO_2 and 4-amino-TEMPO, *ACS Catal.*, 2019, **9**, 10694–10704; (*c*) N. O. Balayeva, Z. Mamiyev, R. Dillert, N. Zheng and D. W. Bahnemann, Rh/TiO_2-photocatalyzed acceptorless dehydrogenation of N-heterocycles upon visible-light illumination, *ACS Catal.*, 2020, **10**, 5542–5553.

30 See, for instance: (*a*) F. Alonso, R. Buitrago, Y. Moglie, A. Sepúlveda-Escribano and M. Yus, Selective hydrosilylation of 1,3-diynes catalyzed by titania-supported platinum, *Organometallics*, 2012, **31**, 2336–2342; (*b*) F. Alonso, Y. Moglie, L. Pastor-Pérez and A. Sepúlveda-Escribano, Solvent- and ligand-free diboration of alkynes and alkenes catalyzed by platinum nanoparticles on titania, *ChemCatChem*, 2014, **6**, 857–865; (*c*) I. Martín-García and F. Alonso, Synthesis of dihydroindoloisoquinolines through the copper-catalyzed cross-dehydrogenative coupling of tetrahydroisoquinolines and nitroalkanes, *Chem.–Eur. J.*, 2018, **24**, 18857–18862; (*d*) A. V. Sirotkin, M. Radosová, A. Tarko, I. Martín-García and F. Alonso, Effect of morphology and support of copper nanoparticles on basic ovarian granulosa cell functions, *Nanotoxicology*, 2020, **14**, 683–695.

31 For selected references, see: (*a*) S. P. Pitre, T. P. Yoon and J. C. Scaiano, Titanium dioxide visible light photocatalysis: surface association enables photocatalysis with visible light irradiation, *Chem. Commun.*, 2017, **53**, 4335–4338; (*b*) A. Hainer, N. Marina, S. Rincon, P. Costa, A. Lanterna and J. C. Scaiano, Highly electrophilic titania hole as a versatile and efficient photochemical free radical source, *J. Am. Chem. Soc.*, 2019, **141**, 4531–4535; (*c*) A. Elhage, A. E. Lanterna and J. C. Scaiano, Catalytic farming: reaction rotation extends catalyst performance, *Chem. Sci.*, 2019, **10**, 1419–1425; (*d*) I. D. Lemir, J. E. Arguello, A. E. Lanterna and J. C. Scaiano, Heterogeneous photocatalysis of azides: extending nitrene photochemistry to longer wavelengths, *Chem. Commun.*, 2020, **56**, 10239–10242.

32 I. Martín-García, G. Díaz-Reyes, G. Sloan, Y. Moglie and F. Alonso, Sulfur-stabilised copper nanoparticles for the aerobic oxidation of amines to imines under ambient conditions, *J. Mater. Chem. A*, 2021, **9**, 11312–11322.

33 M. Yaghmaei, M. Villanueva, I. Martín-García, F. Alonso, X. Zhang, N. Joshi, A. E. Lanterna and J. C. Scaiano, Photosensitised selective semi-oxidation of tetrahydroisoquinoline: A singlet oxygen path, *Photochem. Photobiol. Sci.*, 2022, **21**, 1473–1479.

34 (*a*) *Nanomaterials for Photocatalytic Chemistry*, ed. Y. Sun, World Scientific, New Jersey, 2017; (*b*) C. Xu, P. R. Anusuyadevi, C. Aymonier, R. Luque and S. Marre, Nanostructured materials for photocatalysis, *Chem. Soc. Rev.*, 2019, **48**, 3868–3902.

35 (*a*) Y. Mi and T. Weng, Band alignment and controllable electron migration between rutile and anatase TiO_2, *Sci. Rep.*, 2015, **5**, 11482; (*b*) C. Maheu, L. Cardenas, E. Puzenat, P. Afanasiev and C. Geantet, UPS and UV spectroscopies combined to position the energy levels of TiO_2 anatase and rutile nanopowders, *Phys. Chem. Chem. Phys.*, 2018, **20**, 25629–25637.

36 Review: V. Etacheri, C. Di Valentin, J. Schneider, D. Bahnemann and S. C. Pillai, Visible-light activation of TiO_2 photocatalysts: Advances in theory and experiments, *J. Photochem. Photobiol. C Photochem. Rev.*, 2015, **25**, 1–29.

37 (*a*) F. Alonso, J. J. Calvino, I. Osante and M. Yus, A new straightforward and mild preparation of nickel(0) nanoparticles, *Chem. Lett.*, 2005, **34**, 1262–1263; (*b*) For a former account, see: F. Alonso and M. Yus, New synthetic methodologies based on active transition metals, *Pure Appl. Chem.*, 2008, **80**, 1005–1012.

38 (*a*) M. Faisal, F. A. Harraz, A. A. Ismail, A. M. El-Toni, S. A. Al-Sayari, A. Al-Hajry and M. S. Al-Assiri, Novel mesoporous NiO/TiO_2 nanocomposites with enhanced photocatalytic activity under visible light illumination, *Ceram. Int.*, 2018, **44**, 7047–7056; (*b*) M. Kunnamareddy, R. Rajendran, M. Sivagnanam, R. Rajendran and B. Diravidamani, Nickel and sulfur codoped TiO_2 nanoparticles for efficient visible light photocatalytic activity, *J. Inorg. Organomet. Polym. Mater.*, 2021, **31**, 2615–2626.

39 G. Wang, L. Xu, J. Zhang, T. Yin and D. Han, Enhanced photocatalytic activity of powders (P25) via calcination treatment, *Int. J. Photoenergy*, 2012, e265760.

40 M. Thommes, K. Kaneko, A. V. Neimark, J. P. Olivier, F. Rodriguez-Reinoso, J. Rouquerol and K. S. W. Sing, Physisorption of gases, with special reference to the evaluation of surface area and pore size distribution (IUPAC Technical Report), *Pure Appl. Chem.*, 2015, **87**, 1051–1069.

41 Evonik Operations GmbH, Product information AEROXIDE® TiO_2 P25, Apr 2021: BET = 35–65 $m^2\ g^{-1}$.

42 T. Kodom, G. Djanuje-Boundjou, L. M. Bawa, B. Gombert and N. Alonso-Cante, Etude de la photodégradation du reactive black 5 et du reactive orange 16 en solution aqueuse en utilisant des couches minces de TiO_2, *Int. J. Biol. Chem. Sci.*, 2011, **5**, 232–246.

43 L.-C. Chen, C.-C. Chen, K.-C. Liang, S. H. Chang, Z.-L. Tseng, S.-C. Yeh, C.-T. Chen, W.-T. Wu and C.-G. Wu, Nano-structured CuO-Cu_2O complex thin film for application in $CH_3NH_3PbI_3$ perovskite solar cells, *Nanoscale Res. Lett.*, 2016, **11**, 402.

44 L. Clarizia, G. Vitiello, G. Luciani, I. Di Somma, R. Andreozzi and R. Marotta, In situ photodeposited nanoCu on TiO_2 as a catalyst for hydrogen production under UV/visible radiation, *Appl. Catal., A*, 2016, **518**, 142–149.

45 K. V. R. Chary, G. V. Sagar, C. S. Srikanth and V. V. Rao, Characterization and catalytic functionalization of copper oxide catalysts supported on zirconia, *J. Phys. Chem. B*, 2007, **111**, 543–550.

46 In several cases, isolation of the product by column chromatography proved challenging due to partial overlap with residual starting amine and/or minor by-products.

47 (*a*) D. Prat, J. Haylerb and A. Wells, A survey of solvent selection guides, *Green Chem.*, 2014, **16**, 4546–4551; (*b*) H. E. Eastman, C. Jamieson and A. J. B. Watson, Development of Solvent Selection Guides, *Aldrichimica Acta*, 2015, **48**, 51–55; (*c*) D. Prat, A. Wells, J. Hayler, H. Sneddon, C. R. McElroy, S. Abou-Shehada and P. J. Dunne, CHEM21 selection guide of classical- and less classical-solvents, *Green Chem.*, 2016, **18**, 288–296.

48 (*a*) R. A. Sheldon, The E-factor 25 years on: the rise of green chemistry and sustainability, *Green Chem.*, 2017, **19**, 18–43; (*b*) A. Quintavalla, D. Carboni and M. Lombardo, Green metrics and sustainability in photocatalysis, *ChemCatChem*, 2024, **16**, e202301225.

49 T. P. Yoon, J. C. Scaiano and S. P. Pitre, Photocatalytic indole Diels-Alder cycloadditions mediated by heterogeneous platinum-modified titanium dioxide, *ACS Catal.*, 2017, **7**, 6440–6444.

50 A. Burg and D. Meyerstein, The chemistry of monovalent copper in aqueous solutions, *Adv. Inorg. Chem.*, 2012, **64**, 219–261.

51 M. A. Cismesia and T. P. Yoon, Characterizing chain processes in visible light photoredox catalysis, *Chem. Sci.*, 2015, **6**, 5426–5434.

52 Minireview: M. Muscetta, R. Andreozzi, L. Clarizia, I. Di Somma and R. Marotta, Hydrogen production through photoreforming processes over Cu_2O/TiO_2 composite materials: A mini-review, *Int. J. Hydrogen Energy*, 2020, **45**, 28531–28552.

53 L. Huang, F. Peng, H. Wang, H. Yu and Z. Li, Preparation and characterization of Cu_2O/TiO_2 nano–nano heterostructure photocatalysts, *Catal. Commun.*, 2009, **10**, 1839–1843.

54 L. Clarizia, G. Vitiello, D. K. Pallotti, B. Silvestri, M. Nadagouda, S. Lettieri, G. Luciani, R. Andreozzi, P. Maddalena and R. Marotta, Effect of surface properties of copper-modified commercial titanium dioxide photocatalysts on hydrogen production through photoreforming of alcohols, *Int. J. Hydrogen Energy*, 2017, **42**, 28349–28362.

55 P. Jessop, Evidence of a significant advance in green chemistry, *Green Chem.*, 2020, **22**, 13–15.

56 Safety Data Sheet, Sigma-Aldrich (19-12-2024).

57 Safety Data Sheet, Evonik (08-03-2024).